Some recent Finite Volume schemes to compute Euler equations using real gas EOS

Thierry Gallouët, Jean-Marc Hérard, Nicolas Seguin

Centre de Mathématique et Informatique
Université de Provence
39 rue Joliot Curie. 13453 MARSEILLE Cedex 13

Abstract

This paper deals with the resolution by Finite Volume methods of Euler equations in one space dimension, with real gas state laws (namely perfect gas EOS, Tammann EOS and Van Der Waals EOS). All tests are of shock tube type, in order to examine a wide class of solutions, involving Sod shock tube, stationary shock wave, unsteady contact discontinuity, occurence of vacuum by double rarefaction wave, propagation of a 1-rarefaction wave over "vacuum", ... Most of methods computed herein are approximate Godunov solvers : VFRoe, VFFC, VFRoe ncv (τ, u, p) and PVRS. The energy relaxation method with VFRoe ncv (τ, u, p) and Rusanov scheme have been investigated too. Qualitative results are presented or commented for all test cases and numerical rates of convergence on some test cases have been measured for first and second order (Runge-Kutta 2 with MUSCL reconstruction) approximations.

We discuss in this paper the suitability of some Finite Volume schemes to compute Euler equations when dealing with real gas state laws, restricting to the one dimensional framework. Some measured rates of convergence will be presented when focusing on some Riemann problem test cases. This work is based on [40].

Almost all schemes investigated here are approximate Riemann solvers (more exactly approximate Godunov solvers). One may note that comparison with some well known schemes like Godunov scheme or Roe scheme are not provided in this paper ; however, one may refer to [7], [25], [31], [32], [45] for that purpose. Approximate Riemann solvers presented herein may be derived using the general formalism of VFRoe ncv scheme. This only requires defining some suitable variable which is not necessarily the conservative variable, but may be defined on the basis of the solution of the Riemann problem for instance. The first one is obviously VFRoe scheme introduced in [17],[31] and [32], where the candidate is the conservative variable. In the second one, which is known as VFFC scheme, and was introduced in [19], [2] and [29], the privileged variable is the flux variable. The third one, which was introduced some years ago in [6] and with more details in [9], suggests to consider the (τ, u, p) variable in the Euler framework. Extensions of the latter scheme to the frame of shallow water equations, or to some non conservative hyperbolic systems arising in the "turbulent" literature are described in [5], [7] and [8]. The fourth one, which applies for the (ρ, u, p) variable when computing the Euler equations , was introduced by E. F. Toro in [41], [42] and [27], and is known as PVRS (Primitive Variable Riemann Solver). Note that the latter two rely on (u, p) components, which completely determine the solution of the associated Riemann problem, in the sense that assuming no jump on these in the initial conditions results in "ghost" 1-wave and 3-wave. Thus the latter two schemes, which are based on the use of u and p variables, are indeed quite different from the other two, since the former require no knowledge of the one dimensional Riemann problem solution.

Two slightly different schemes are also used for broader comparison. The first one is the Rusanov scheme ([36]), which is known to be rather "diffusive" but anyway enjoys rather pleasant properties, especially when one aims at computing multi dimensional flows on any kind of unstructured mesh. Recall that for Euler type systems, this scheme ensures the positivity of mass and species, provided that the "cell" CFL number is smaller than 1 ([18]). Even more, it requires no entropy correction at sonic points in rarefaction waves, when restricting to "first" order formulation. The last scheme examined is the energy relaxation method proposed by F. Coquel and B. Perthame in [13] (see also [26] and [25] for applications) applied to the frame of VFRoe scheme with (τ, u, p) variable. This one again seems appealing both for its simplicity and for its ability to get rid of entropy correction at sonic points in regular fields.

Both "first order" schemes and "second order" schemes (using RK2 time integration and MUSCL reconstruction with minmod limiter on primitive variables) are examined. This includes three distinct EOS, namely :
- perfect gas EOS
- Van der Waals EOS

- Tammann EOS

Though complex tabulated EOS are not discussed herein, all above mentionned schemes enable computation of EOS such as those detailed in [34] or [28]. Numerical experiments involve a wide variety of initial conditions, so that the solution may be either a 1-rarefaction wave with a 3- shock wave, a double shock wave or a double rarefaction wave. We give emphasis on symetric double rarefaction (or shock) waves, since these allow investigation of wall boundary conditions when the standard mirror technique is applied for. The particular experiment of a single isolated contact discontinuity is also described, since the behaviour highly depends on the nature of the state law (see also [39] on that specific topic). Note also that for almost incompressible fluids, the eigenvalue associated with the LD field is such that the local CFL number varies as $M/(1+M)$, where M stands for the local Mach number, as soon as the overall CFL number is set to 1. As a result, the accuracy of the prediction of the contact discontinuity is rather poor, which is rather annoying since the vapour quality only varies through this field. Eventually, we note that these test cases include the occurence of vacuum, and the propagation of a shock wave over a (almost) vacuum of gas. The standard stationnary shock is also reported. For completness, we also refer to [30] where Godunov scheme [21] is used to compute Van Der Waals EOS.

Qualitative behaviour of schemes is discussed, and L^1 error norm is plotted in some cases to provide quantitative comparison.

1 Governing equations

1.1 Euler equations under conservative form

Governing Euler equations are written in terms of the mean density ρ, the mean pressure P, the mean velocity u and the total energy E as follows:

$$\frac{\partial W}{\partial t} + \frac{\partial F(W)}{\partial x} = 0 \tag{1}$$

setting :

$$W = \begin{pmatrix} \rho \\ \rho u \\ E \end{pmatrix} \quad , \quad F(W) = \begin{pmatrix} \rho u \\ \rho u^2 + p \\ u(E+p) \end{pmatrix} \quad \text{and} \quad E = \rho(\frac{1}{2}u^2 + \varepsilon)$$

If ε denotes the internal energy, then some law is required to close the whole system:

$$p = p(\rho, \varepsilon) \tag{2}$$

such that the Jacobian matrix may be diagonalized in $\mathbb{R}$ for $W \in \Omega$, Ω the set of admissible states, so that $\hat{\gamma}(p,\rho)p > 0$, $\rho > 0$, where :

$$\rho c^2(p,\rho) = \hat{\gamma}(p,\rho)p = \left(\frac{\partial \varepsilon}{\partial p}_{|\rho}\right)^{-1} \left(\frac{p}{\rho} - \rho \frac{\partial \varepsilon}{\partial \rho}_{|p}\right)$$

Herein, c stands for the speed of acoustic waves.

The Jacobian matrix $A(W) = \dfrac{\partial F(W)}{\partial W}$ may be written :

$$A(W) = \begin{pmatrix} 0 & 1 & 0 \\ K - u^2 & u(2-k) & k \\ (K-H)u & H - ku^2 & u(1+k) \end{pmatrix}$$

setting:

$$\begin{aligned} H &= \frac{E+p}{\rho} \\ k &= \frac{1}{\rho}\frac{\partial p}{\partial \varepsilon}_{|\rho} \\ K &= c^2 + k(u^2 - H) \end{aligned}$$

Eigenvalues of the Jacobian matrix $A(W)$ read :

$$\lambda_1 = u - c,\ \lambda_2 = u,\ \lambda_3 = u + c$$

Associated right eigenvectors are :

$$r_1(W) = \begin{pmatrix} 1 \\ u - c \\ H - uc \end{pmatrix},\ r_2(W) = \begin{pmatrix} 1 \\ u \\ H - \frac{c^2}{k} \end{pmatrix},\ r_3(W) = \begin{pmatrix} 1 \\ u + c \\ H + uc \end{pmatrix}$$

Left eigenvectors of $A(W)$ are :

$$l_1(W) = \frac{1}{2c^2}\begin{pmatrix} K + uc \\ -ku - c \\ k \end{pmatrix},\ l_2(W) = \frac{k}{c^2}\begin{pmatrix} H - u^2 \\ u \\ -1 \end{pmatrix},\ l_3(W) = \frac{1}{2c^2}\begin{pmatrix} K - uc \\ -ku + c \\ k \end{pmatrix}$$

Recall that the 1-wave and the 3-wave are Genuinely Non Linear fields and that the 2-wave is Linearly Degenerated. In an alternative way, Euler equations may be written in a non conservative form, when restricting to smooth solutions.

We only provide herein some useful computations of right and left eigenvectors based on non conservative forms of Euler equations.

1.2 Non conservative form wrt (τ, u, p)

Let us set $\tau = 1/\rho$. Thus, Euler equations may written in terms of (τ, u, p) as :

$$\frac{\partial Y_1}{\partial t} + B_1(Y_1)\frac{\partial Y_1}{\partial x} = 0$$

with

$$Y_1 = \begin{pmatrix} \tau \\ u \\ p \end{pmatrix} \quad \text{and} \quad B_1(Y_1) = \begin{pmatrix} u & -\tau & 0 \\ 0 & u & \tau \\ 0 & \hat{\gamma}p & u \end{pmatrix}$$

Obviously, eigenvalues of $B_1(Y_1)$ are still :

$$\lambda_1 = u - c,\ \lambda_2 = u,\ \lambda_3 = u + c$$

Right eigenvectors of matrix $B_1(Y_1)$ are :

$$r_1(Y_1) = \begin{pmatrix} \tau \\ c \\ -\hat{\gamma}p \end{pmatrix}, \; r_2(Y_1) = \begin{pmatrix} 1 \\ 0 \\ 0 \end{pmatrix}, \; r_3(Y_1) = \begin{pmatrix} \tau \\ -c \\ -\hat{\gamma}p \end{pmatrix}$$

Left eigenvectors of $B_1(Y_1)$ are :

$$l_1(Y_1) = \frac{1}{2c^2}\begin{pmatrix} 0 \\ c \\ -\tau \end{pmatrix}, \; l_2(Y_1) = \frac{1}{c^2}\begin{pmatrix} 1 \\ 0 \\ \tau^2 \end{pmatrix}, \; l_3(Y_1) = \frac{1}{2c^2}\begin{pmatrix} 0 \\ -c \\ -\tau \end{pmatrix}$$

1.3 Non conservative form wrt (ρ, u, p)

In a similar way, we may rewrite Euler equations in terms of (ρ, u, p) :

$$\frac{\partial Y_2}{\partial t} + B_2(Y_2)\frac{\partial Y_2}{\partial x} = 0$$

with:

$$Y_2 = \begin{pmatrix} \rho \\ u \\ p \end{pmatrix} \quad \text{et} \quad B_2(Y_2) = \begin{pmatrix} u & \rho & 0 \\ 0 & u & \frac{1}{\rho} \\ 0 & \hat{\gamma}p & u \end{pmatrix}$$

Right eigenvectors of $B_2(Y_2)$ are now :

$$r_1(Y_2) = \begin{pmatrix} 1 \\ -\frac{c}{\rho} \\ c^2 \end{pmatrix}, \; r_2(Y_2) = \begin{pmatrix} 1 \\ 0 \\ 0 \end{pmatrix}, \; r_3(Y_2) = \begin{pmatrix} 1 \\ \frac{c}{\rho} \\ c^2 \end{pmatrix}$$

Meanwhile, left eigenvectors of matrix $B_2(Y_2)$ read :

$$l_1(Y_2) = \frac{1}{2c^2}\begin{pmatrix} 0 \\ -\rho c \\ 1 \end{pmatrix}, \; l_2(Y_2) = \begin{pmatrix} 1 \\ 0 \\ -\frac{1}{c^2} \end{pmatrix}, \; l_3(Y_2) = \frac{1}{2c^2}\begin{pmatrix} 0 \\ \rho c \\ 1 \end{pmatrix}$$

1.4 Non conservative form wrt $F(W)$

We may rewrite the above mentionned equations in terms of variable $Y = F(W)$. We multiply on the left by $A(W)$ system (1) :

$$A(W)\frac{\partial W}{\partial t} + A(W)\frac{\partial F(W)}{\partial x} = 0$$

Since $A(W)$ is the Jacobian matrix of flux $F(W)$, we get :

$$A(W)\frac{\partial W}{\partial t} = \frac{\partial F(W)}{\partial t}$$

Hence:

$$\frac{\partial F(W)}{\partial t} + A(W)\frac{\partial F(W)}{\partial x} = 0$$

The associated matrix still is $A(W)$. Eigenstructure is detailed in 1.1. We now describe the three equations of state used in our computations.

1.5 Considering various EOS

1.5.1 Perfect gas EOS

The closure law is :

$$p = (\gamma - 1)\rho\varepsilon$$

with:

$$\gamma = 1,4$$

1.5.2 Tammann EOS

This law is sometimes used to describe the thermodynamics of the liquid phase (see [41]). It may be simply written as :

$$p = (\gamma_c - 1)\rho\varepsilon - \gamma_c p_c$$

where:

$$\gamma_c = 7,15 \quad p_c = 3.10^8$$

Actually, using some suitable change of variables enables to retrieve Euler equations with perfect gas state law, assuming $\gamma = \gamma_c$. This is an interesting point, since some schemes benefit from nice properties when restricting to perfect gas EOS (see for instance VFRoe with non conservative variable).

1.5.3 Van Der Waals EOS

Van Der Waals EOS is recalled below: :

$$(p + \frac{a}{\tau^2})(\tau - b) = RT$$
$$\varepsilon - \varepsilon_0 = c_v T - \frac{a}{\tau}$$
$$c^2 = -2\frac{a}{\tau} + (p\tau^2 + a)(1 + \frac{R}{c_v})/(\tau - b)$$

where:

$$\begin{array}{rclrcl} b & = & 0,001692 & R & = & 461,5 \\ a & = & 1684,54 & c_v & = & 1401,88 \\ \varepsilon_0 & = & 0 & & & \end{array}$$

This identifies with perfect gas EOS while setting $a = b = 0$. This law enables to exhibit some deficiencies of schemes around the contact discontinuity in some cases. We refer to [30] which provides some approximation based on Godunov scheme, when focusing on this particular EOS. Initial conditions in shock-tube experiments are taken in this reference. Comparison with some other test cases can be found in [18], [6] and [9].

2 Numerical schemes

2.1 Framework

2.1.1 Finite Volume schemes

We thus focus herein on some Finite Volume schemes (see for example [20] and [15]). Regular meshes are considered, whose size Δx is such that: $\Delta x = x_{i+\frac{1}{2}} - x_{i-\frac{1}{2}}$, $i \in \mathbb{Z}$. Let us denote as usual Δt the time step, where $\Delta t = t^{n+1} - t^n$, $n \in \mathbb{N}$.
We denote $W \in \mathbb{R}^n$ the exact solution of the non degenerate hyperbolic system :

$$\left\{ \begin{array}{l} \dfrac{\partial W}{\partial t} + \dfrac{\partial F(W)}{\partial x} = 0 \\ W(x,0) = W_0(x) \end{array} \right.$$

with $F(W)$ in $\mathbb{R}^n$.
Let W_i^n be the approximate value of $\dfrac{1}{\Delta x} \displaystyle\int_{x_{i-\frac{1}{2}}}^{x_{i+\frac{1}{2}}} W(x,t^n)dx$.
Integrating over $[x_{i-\frac{1}{2}}; x_{i+\frac{1}{2}}] \times [t^n; t^{n+1}]$ provides:

$$W_i^{n+1} = W_i^n - \frac{\Delta t}{\Delta x}\left(\phi_{i+\frac{1}{2}}^n - \phi_{i-\frac{1}{2}}^n\right)$$

where $\phi_{i+\frac{1}{2}}^n$ is the numerical flux through the interface $\{x_{i+\frac{1}{2}}\} \times [t^n; t^{n+1}]$. The time step should comply with some CFL condition in order to guarantee non interaction of numerical waves inside one particular cell, or some other stability requirement. We restrict our presentation to the frame of three point schemes. Thus $\phi_{i+\frac{1}{2}}^n$ only depends on W_i^n et W_{i+1}^n, namely $\phi_{i+\frac{1}{2}}^n = \phi(W_i^n, W_{i+1}^n)$. Whatever the scheme is, the following consistancy relation should hold :

$$\phi(V,V) = F(V)$$

Hence, we present now approximate numerical fluxes $\phi(W_L, W_R)$ associated with the 1D Riemann problem :

$$\left\{ \begin{array}{l} \dfrac{\partial W}{\partial t} + \dfrac{\partial F(W)}{\partial x} = 0 \\ W(x,0) = \left\{ \begin{array}{ll} W_L & \text{if } x < 0 \\ W_R & \text{if } x > 0 \end{array} \right. \end{array} \right. \tag{3}$$

2.1.2 VFRoe schemes

These are approximate Godunov schemes where the approximate value at the interface between two cells is computed as follows. Let us consider some change of variable $Y = Y(W)$ in such a way that $W_{,Y}(Y)$ is inversible. The counterpart of above system for regular solutions is :

$$\frac{\partial Y}{\partial t} + B(Y)\frac{\partial Y}{\partial x} = 0$$

where $B(Y) = (W_{,Y}(Y))^{-1} A(W(Y))\ W_{,Y}(Y)$ ($A(W)$ stands for the jacobian matrix of flux $F(W)$).
Now, the numerical flux $\phi(W_L, W_R)$ is obtained solving the linearized hyperbolic system :

$$\left\{ \begin{array}{l} \dfrac{\partial Y}{\partial t} + B(\hat{Y}) \dfrac{\partial Y}{\partial x} = 0 \\ Y(x,0) = \left\{ \begin{array}{ll} Y_L = Y(W_L) & \text{if } x < 0 \\ Y_R = Y(W_R) & \text{if } x > 0 \end{array} \right. \end{array} \right. \tag{4}$$

where $\hat{Y}$ agrees with condition: $\hat{Y}(Y_L, Y_L) = Y_L$.

Once the exact solution $Y^*(\frac{x}{t}; Y_L, Y_R)$ of this approximate problem is obtained, the numerical flux is :

$$\phi(W_L, W_R) = F(W(Y^*(0; Y_L, Y_R)))$$

Notation *In the following we note ˜ variables which are computed on the basis of $\overline{Y}$ (obviously, if α is one component of $\overline{Y}$, the relation below holds: $\widetilde{\alpha} = \overline{\alpha}$).*

Let us set $\widetilde{l_k}$, $\widetilde{\lambda_k}$ and $\widetilde{r_k}$, $k = 1, ..., n$, left eigenvectors and eigenvalues of matrix $B(\overline{Y})$ respectively. The solution $Y^*(\frac{x}{t}; Y_L, Y_R)$ of linear problem is :

$$\begin{aligned} Y^*\left(\frac{x}{t}; Y_L, Y_R\right) &= Y_L + \sum_{\frac{x}{t} < \widetilde{\lambda_k}} ({}^t\widetilde{l_k}.(Y_R - Y_L))\widetilde{r_k} \\ &= Y_R - \sum_{\frac{x}{t} > \widetilde{\lambda_k}} ({}^t\widetilde{l_k}.(Y_R - Y_L))\widetilde{r_k} \end{aligned}$$

2.1.3 Entropy correction

When one numerical eigenvalue associated with the 1-wave or the 3-wave vanishes, an entropy correction is needed for above mentionned schemes, when restricting to three point schemes (eg without any MUSCL type reconstruction). If a 1-rarefaction wave overlapping the interface is detected, the approximate value at the interface is modified as:

$$Y^*(0; Y_L, Y_R) = \frac{Y_L + Y_1}{2}$$

In a first approach ([6]), we may assume that overlapping occurs if :

$$\lambda_1(W_L) < 0$$

and if in addition $\widetilde{\lambda_1}$ is close to 0.

An alternative way consists in the proposal of A. Harten and J.M. Hyman in [22], thus checking whether :

$$\lambda_1(W_L) < 0 < \lambda_1(W_R)$$

This second approach has been applied herein.

2.2 Basic VFRoe scheme

This scheme was first proposed in [17], [31] and [32]. It is based on the following choice $Y(W) = W$ and thus $B(\overline{Y}) = A(\overline{W})$. Recall that $A(W)$ is the Jacobian matrix of $F(W)$ in the linearized Riemann problem.

2.3 VFRoe with non conservative variable (τ, u, p)

We set now $Y(W) = {}^t(\tau, u, p)$, where $\tau = 1/\rho$. This scheme was introduced in [6] (see also [9] and [7], [18], [8] for various applications).

With help of left eigenvectors of $B(\overline{Y})$ detailed in 1.2 , and defining $\tilde{\alpha}_1$ and $\tilde{\alpha}_3$ as :

$$\tilde{\alpha}_1 = \frac{1}{2\widetilde{c^2}}(\widetilde{c}\Delta u - \overline{\tau}\Delta p)$$
$$\tilde{\alpha}_3 = -\frac{1}{2\widetilde{c^2}}(\widetilde{c}\Delta u + \overline{\tau}\Delta p)$$

where $\Delta(.) = (.)_R - (.)_L$, intermediate states Y_1 and Y_2 read :

$$Y_1 = \begin{pmatrix} \tau_L + \tilde{\alpha}_1\overline{\tau} \\ u_L + \tilde{\alpha}_1\widetilde{c} \\ p_L - \tilde{\alpha}_1\widetilde{\gamma}\overline{p} \end{pmatrix} \qquad \text{and} \qquad Y_2 = \begin{pmatrix} \tau_R - \tilde{\alpha}_3\overline{\tau} \\ u_R + \tilde{\alpha}_3\widetilde{c} \\ p_R + \tilde{\alpha}_3\widetilde{\gamma}\overline{p} \end{pmatrix}$$

Now:

$$Y_2 = Y_1 + ({}^t\widetilde{l}_2.(Y_R - Y_L))\widetilde{r}_2$$

and last composants of $\widetilde{r_2}$ are null, hence $u_1 = u_2$ and $p_1 = p_2$. The approximate solution is thus in agreement with the exact solution of the Riemann problem. Even more, if we assume that initial conditions agree with $\Delta u = 0$ and $\Delta p = 0$, the following holds $Y_1 = Y_L$ and $Y_2 = Y_R$ (see [9]). This results in the fact that for some particular EOS such as perfect gas EOS and Tammann EOS, cell averages of velocity and pressure are perfectly preserved through the 2-wave, when focusing on single moving contact discontinuity and scheme VFRoe ncv (τ, u, p) (see [8] and appendix A for a general expression of the EOS).

Another property of this scheme is that single 1-shocks (respectively 3-shocks) are preserved in the sense that exact jump conditions and approximate jump conditions arising from linearised system are equivalent, when restricting to perfect gas EOS. In other words, if we set σ the speed of the shock wave and $[\alpha]$ the jump of α through this shock wave, then :

$$-\sigma[W] + [F(W)] = 0$$

and :

$$-\sigma[Y] + B(\overline{Y})[Y] = 0$$

are the same (see [9] for more details). However, note that this scheme does not fulfill the Roe condition (see [35]).

Eventually, we note that strictly speaking, the value $\widetilde{\gamma}$ is completely determined for given choice of Y. Details concerning the discrete preservation of the positivity of density and pressure intermediate states can be found in [9].

2.4 VFRoe with non conservative variable (ρ, u, p) -PVRS-

We now set $Y(W) = {}^t(\rho, u, p)$. This scheme actually identifies with PVRS (Primitive Variable Riemann Solver) scheme proposed by E.F. Toro, in [42] or [27]. Coefficients $\tilde{\alpha}_1$ and $\tilde{\alpha}_3$ are now :

$$\tilde{\alpha}_1 = \frac{1}{2\tilde{c}^2}(-\overline{\rho}\tilde{c}\Delta u + \Delta p)$$

$$\tilde{\alpha}_3 = \frac{1}{2\tilde{c}^2}(\overline{\rho}\tilde{c}\Delta u + \Delta p)$$

Hence :

$$Y_1 = \begin{pmatrix} \rho_L + \tilde{\alpha}_1 \\ u_L - \tilde{\alpha}_1 \frac{\tilde{c}}{\overline{\rho}} \\ p_L + \tilde{\alpha}_1 \tilde{c}^2 \end{pmatrix} \qquad \text{and} \qquad Y_2 = \begin{pmatrix} \rho_R - \tilde{\alpha}_3 \\ u_R - \tilde{\alpha}_3 \frac{\tilde{c}}{\overline{\rho}} \\ p_R - \tilde{\alpha}_3 \tilde{c}^2 \end{pmatrix}$$

Once again, we check that :

$$Y_2 = Y_1 + ({}^t\tilde{l}_2.(Y_R - Y_L))\tilde{r}_2$$

so that approximate intermediate states mimic the behaviour of the exact Godunov scheme. Moreover, for perfect gas EOS and Tamman EOS, cell averages of Riemann invariants of the 2-wave are perfectly preserved. Above mentionned remark concerning jump conditions no longer holds, even when restricting to perfect gas EOS.

If we turn now to intermediate states of pressure, we note that PVRS scheme computes:

$$p_1 = p_2 = \overline{p}(1 - \frac{\hat{\gamma}(\overline{p}, \overline{\rho})\Delta u}{2\tilde{c}})$$

Thus the pressure intermediate states are strictly positive as soon as:

$$\frac{\Delta u}{\tilde{c}} < \frac{2}{\hat{\gamma}(\overline{p}, \overline{\rho})}$$

This should be compared with continuous condition for vacuum occurence :

$$\Delta u < X_L + X_R \tag{5}$$

where :

$$X_i = \int_0^{\rho_i} \frac{c(\rho, s_i)}{\rho} d\rho$$

where s_i denotes the specific entropy. Thus if we restrict to some symetrical double rarefaction wave with perfect gas EOS, we note that the upper bound of $\frac{\Delta u}{\tilde{c}}$ to avoid occurence of vacuum is $\frac{4}{\gamma - 1}$ in the "continuous case" and $\frac{2}{\gamma}$ in the "discrete case" for PVRS scheme. Using the standard value $\gamma = 1.4$ provides 10 and $\frac{10}{7}$ respectively.

2.5 VFRoe scheme with flux variable -VFFC-

This corresponds to the choice : $Y(W) = F(W)$. This scheme VFFC was first introduced in [19] (see also [2] and [29] for further details). The associated 1D Riemann problem is now :

$$\left\{ \begin{array}{l} \dfrac{\partial F(W)}{\partial t} + A(\overline{W}) \dfrac{\partial F(W)}{\partial x} = 0 \\ F(W(x,0)) = \left\{ \begin{array}{ll} F_L = F(W_L) & \text{if } x < 0 \\ F_R = F(W_R) & \text{if } x > 0 \end{array} \right. \end{array} \right.$$

The interface numerical flux F^* is computed with help of eigenstructure of the Jacobian matrix $A(\overline{W})$, as occurs when focusing on basic VFRoe scheme.

2.6 Rusanov scheme

Unlike schemes presented above, Rusanov scheme do not solve an approximate Riemann problem at each interface (see [36]). Numerical flux of Rusanov scheme is :

$$\phi(W_L, W_R) = \frac{F(W_L) + F(W_R)}{2} - \frac{1}{2} \lambda_{i+\frac{1}{2}}^{MAX} (W_R - W_L)$$

with

$$\lambda_{i+\frac{1}{2}}^{MAX} = \max(|u_L| + c_L, |u_R| + c_R)$$

The mean density remains positive as soon as the C.F.L. condition below holds (see [18] for more details) :

$$\max_{j \in \mathbb{Z}} (|u_j^n| + c_j^n) \Delta t \leq \Delta x$$

Note that a similar condition is exhibited in [40] for the Rusanov scheme with a MUSCL reconstruction with minmod slope limiter ([44]).

2.7 Energy relaxation method applied to VFRoe with non conservative variable (τ, u, p)

The energy relaxation method was introduced in [13], and used in [25] and [26]. We refer to these references for further details, and only provide herein an algorithmic version to compute the flux ϕ, resolving the Riemann problem (3) for the Euler equations.

This requires introducing two additional variables γ_1 and ε_2 to the conservative ones. Coefficent γ_1 must fulfill the following conditions to reach convergence of the energy relaxation method :

$$\gamma_1 > \sup_{\rho, \varepsilon} \Gamma(\rho, \varepsilon) \quad \text{where} \quad \Gamma(\rho, \varepsilon) = 1 + \frac{p_{,\varepsilon}}{\rho} \tag{6}$$

$$\gamma_1 > \sup_{\rho, \varepsilon} \gamma(\rho, \varepsilon) \quad \text{where} \quad \gamma(\rho, \varepsilon) = \frac{\rho}{p} p_{,\rho} + \frac{p_{,\varepsilon}}{\rho} \tag{7}$$

where $\varepsilon = E - \frac{1}{2}\frac{(\rho u)^2}{\rho^2}$ and p is computed using the real EOS (2).
Internal energy ε_2 is defined as follows :

$$\varepsilon_2 = \frac{E}{\rho} - \frac{1}{2}\frac{(\rho u)^2}{\rho^2} - \frac{p}{(\gamma_1 - 1)\rho}$$

We may introduce :

$$W_1(\rho, u, p) = \begin{pmatrix} \rho \\ \rho u \\ \frac{1}{2}\rho u^2 + \frac{p}{\gamma_1 - 1} \end{pmatrix}$$

and:

$$F_1(W_1(\rho, u, p)) = \begin{pmatrix} \rho u \\ \rho u^2 + p \\ u(\frac{1}{2}\rho u^2 + \gamma_1 \frac{p}{\gamma_1 - 1}) \end{pmatrix}$$

The four governing equations are :

$$\begin{cases} \dfrac{\partial W_1}{\partial t} + \dfrac{\partial F_1(W_1)}{\partial x} = 0 \\ (\rho\varepsilon_2)_{,t} + (\rho u \varepsilon_2)_{,x} = 0 \end{cases} \tag{8}$$

with given initial condition :

$${}^t(\rho, u, p, \varepsilon_2)(x, 0) = \begin{cases} {}^t(\rho_L, u_L, p_L, \varepsilon_{2L}) & \text{if } x < 0 \\ {}^t(\rho_R, u_R, p_R, \varepsilon_{2R}) & \text{if } x > 0 \end{cases} \tag{9}$$

Thanks to these, one may compute the VFRoe-ncv numerical flux pertaining to the latter system which is an hyperbolic system with three distinct eigenvalues which are those of the Euler system. The numerical flux with three components relative to the mass, momentum and energy equations will eventually be defined as follows :

$$\phi(W_L, W_R) = \begin{pmatrix} F^*_{1,1} \\ F^*_{1,2} \\ F^*_{1,3} + (\rho u \varepsilon_2)^* \end{pmatrix}$$

noting $F^*_1 = {}^t(F^*_{1,1}, F^*_{1,2}, F^*_{1,3})$.
Since we use the VFRoe ncv (τ, u, p) scheme to solve the four equations system, we get :

$$\begin{aligned} (\rho u \varepsilon_2)^* &= \rho^* u^* \varepsilon_{2L} \quad \text{if } \overline{u}_{LR} > 0 \\ &= \rho^* u^* \varepsilon_{2R} \quad \text{if } \overline{u}_{LR} < 0 \end{aligned}$$

Since ε_2 is defined for each Riemann problem resolution, this variable is not continous in time (a jump occurs at each time step).

3 Numerical results

All test cases have been computed for all schemes, but we do not present here all results (see [40], pp.53-451). However, they are all discussed in the following, with some figures to focus on problems in critical configurations. Let us note that VFRoe ncv $(\tau, , u, p)$ scheme without entropy correction have been investigated too, in order to emphasize the influence of the energy relaxation method.

Following tests are performed using constant CFL number ; however, CFL number slightly increases at the beginning of the computation, from $0,1$ to $0,4$ in $t \in [0; T_{MAX}/4]$. Initial conditions refer to different 1D Riemann problems. The regular mesh contains one hundred nodes.

We present results pertaining to perfect gas, focusing first on qualitative behaviour and then on measurement of L^1 error norm of four distinct solutions. After, some qualitative results are discussed, related to the Tammann EOS. The configurations of these test cases are similar to perfect gas EOS. At the end, two cases are presented with the Van Der Waals EOS, in order to emphasize some numerical problems through the LD field.

Remark 1 *Unless otherwise specified, the average of $\hat{\gamma}$ which is used in all test cases is the following: $0.5((\hat{\gamma})_L + (\hat{\gamma})_R)$. The main advantage of this proposal issuing from [6] is that the mean Jacobian matrix has real eigenvalues, provided that initial states have. This is not necessarily true for some non convex EOS when applying for expected value, i.e. : $\widetilde{\hat{\gamma}} = \hat{\gamma}(\overline{Y})$. However, potential drawbacks of the former approach will be discussed when necessary. This remark obviously holds for Tammann EOS and Van der Waals EOS, but not for perfect gas state law.*

3.1 Perfect gas EOS - Qualitative behavior

Case 1.1 Perfect gas EOS - Sod shock tube

A 1-rarefaction wave travels to the left and a 3-shock moves to the right end. The contact discontinuity is right going. This case is usually examined but does not provide much information on schemes since discrepancies can hardly be exhibited between all schemes involved herein. However, one can note that "first-order" Rusanov scheme is a little bit more diffusive than others schemes.

Left State	Right state
$\rho_L = 1$	$\rho_R = 0,125$
$u_L = 0$	$u_R = 0$
$p_L = 10^5$	$p_R = 10^4$

$$T_{MAX} = 6\ ms$$

Case 1.2 Perfect gas EOS - Supersonic 1-rarefaction wave

The 1-rarefaction wave contains a sonic point. As a result, for VFRoe ncv schemes, a wrong shock wave may develop at the origin. This is corrected by introducing an entropy correction at sonic point, when focusing on so called first order scheme. This is no longer compulsory when handling MUSCL type reconstruction, which is usually combined with RK2 time integration in order to avoid loss of stability. Note that VFFC scheme without entropy correction also provides a non entropic shock at sonic point, but this appears to be very small when compared with those arising with VFRoe ncv approach with "physical" variables. Moreover, since the energy relaxation method is applied with VFRoe ncv (τ, u, p) without entropy correction, a small jump can be detected at the sonic point (which vanishes when the mesh is refined). Since first order Rusanov scheme is not based on a linearised Riemann solver, no problem appears at the sonic point. All second order schemes behave in the same way.

Left State	Right state
$\rho_L = 1$	$\rho_R = 0,01$
$u_L = 0$	$u_R = 0$
$p_L = 10^5$	$p_R = 10^3$

$$T_{MAX} = 5\ ms$$

Case 1.3 Perfect gas EOS - Double supersonic rarefaction wave

This case enables to predict the behaviour of the scheme close to wall boundary conditions when applying the mirror technique. Two rarefaction waves are present in the solution when u_R is positive. Due to symetrical initial conditions, the contact discontinuity is a ghost wave. We note that in this particular case VFFC scheme no longer provides a convergent solution since it blows up after a few time steps. Though intermediate states of VFRoe ncv scheme are no longer admissible (see [9]) it however provides a convergent solution. As usual, Rusanov scheme is more diffusive than other schemes, but it provides rather good results.

Left State	Right state
$\rho_L = 1$	$\rho_R = 1$
$u_L = -1200$	$u_R = 1200$
$p_L = 10^5$	$p_R = 10^5$

$$T_{MAX} = 2\ ms$$

Case 1.4 Perfect gas EOS - Double subsonic shock wave

This case is very similar to the previous one, but two shocks are now travelling to the left and to the right since u_R is negative. It corresponds to an inviscid

impinging jet on a wall boundary. For supersonic double shock waves with very high initial kinetic energy, small oscillations may occur close to shocks, even when the CFL number is such that waves do not interact. A similar behaviour is observed when computing the case with help of Godunov scheme. Second order schemes create some oscillations, even in a subsonic configuration, except for Rusanov scheme.

Left State	Right state
$\rho_L = 1$	$\rho_R = 1$
$u_L = 300$	$u_R = -300$
$p_L = 10^5$	$p_R = 10^5$

$$T_{MAX} = 5\ ms$$

Case 1.5 Perfect gas EOS - Stationary 1-shock wave

This case is usually considered to evaluate the stability of the (expected) stationary 1-shock wave, especially when the scheme does not comply with Roe's condition. In all cases, no instability arises, and all schemes (except for the energy relaxation method which inserts two points in the stationary shock wave profile and Rusanov scheme which smears the wave) actually perfectly preserve the steadyness, whatever the order is.

Left State	Right state
$\rho_L = 3/4$	$\rho_R = 1$
$u_L = 4/3$	$u_R = 1$
$p_L = 2/3$	$p_R = 1$

$$T_{MAX} = 100\ s$$

Case 1.6 Perfect gas EOS - Unsteady contact discontinuity

This case is interesting since it enables to check whether the Riemann invariants of the 2-wave are preserved from a discrete point of view. This essentially depends on the scheme and the EOS (see appendix A). All (first and second order) computed schemes preserve velocity and pressure exactly constant, whereas density jump at the contact dicontinuity is smeared. Note that Rusanov scheme is once again more diffusive than schemes based on a linearised Riemann solver and the energy relaxation method.

Left State	Right state
$\rho_L = 1$	$\rho_R = 0,1$
$u_L = 100$	$u_R = 100$
$p_L = 10^5$	$p_R = 10^5$

$$T_{MAX} = 20\ ms$$

Case 1.7 Perfect gas EOS - Supersonic 1-rarefaction wave propagating over "vacuum"

This is one difficult test case for all schemes based on approximate Riemann solvers. Moreover, problems may appear due to the fact that computers have to handle round off errors. The analytical solution is close to a pure 1-rarefaction wave over vacuum, since the variations through the LD field and the 3-shock are not significant. Note that some variables are not defined in vacuum, namely velocity u or specific volume τ. Indeed, for the first order framework, the energy relaxation method applied to VFRoe ncv (τ, u, p) without entropy correction blows up after few time steps. However, VFRoe ncv (τ, u, p) scheme with entropy correction provides good results, except in the vacuum area, where velocity profile becomes less accurate on coarse mesh. Other first order schemes (PVRS, VFFC and Rusanov) provide slightly better profiles, even near vacuum. The second order energy relaxation method and second order VFRoe ncv (τ, u, p) scheme provide good results, though the problem on the velocity profile in the vacuum area remains unchanged. Other second order schemes perform well.

Left State	Right state
$\rho_L = 1$	$\rho_R = 10^{-7}$
$u_L = 0$	$u_R = 0$
$p_L = 10^5$	$p_R = 10^{-2}$

$$T_{MAX} = 1\ ms$$

Case 1.8 Perfect gas EOS - Double rarefaction wave with vacuum

This one too is interesting, since the violation of condition $(\gamma - 1)(u_R - u_L) < 2(c_R + c_L)$ results in a vacuum occurence on each side of the origin. Since this test case provides a double supersonic rarefaction wave, VFFC scheme cannot handle these initial conditions, whatever the order. The energy relaxation method applied to VFRoe ncv (τ, u, p) scheme without entropy correction blows up too, restricting to the first order approximation. However, these two schemes perform well when handling MUSCL reconstruction with RK2 time integration. Moreover, first or second order PVRS, VFRoe and Rusanov schemes preserve density and pressure positivity in this test case and provide good results too (recall that Rusanov scheme maintains positivity of the density under a standard CFL-like condition).

Left State	Right state
$\rho_L = 1$	$\rho_R = 1$
$u_L = -3000$	$u_R = 3000$
$p_L = 10^5$	$p_R = 10^5$

$$T_{MAX} = 1\ ms$$

3.2 Perfect gas EOS - Quantitative behavior

We compute here four test cases (Sod shock tube, supersonic 1-rarefaction wave, double subsonic rarefaction wave and double subsonic shock wave) with several meshes : 100, 300, 1000, 3000 and 10000 nodes. Numerical rates of convergence of the L^1 error are measured and presented. Continous lines represent first order schemes, whereas dotted lines represent second order schemes.

Case 2.1 Perfect gas EOS - Sod shock tube

Initial conditions of this test case are the same as the Case 1.1. Though Rusanov scheme is less accurate than other schemes, its rate of convergence is the same. We can note that the rate of convergence of velocity and pressure are the same and higher than the rate of convergence pertaining to density, owing to the contact discontinuity. As expected, the second order schemes converge faster (the slope is close to 1 for velocity and pressure).

Case 2.2 Perfect gas EOS - Supersonic 1-rarefaction wave

This refers to the Case 1.2. Though the solution of this test case is composed by the same set of waves, we can measure here the influence of entropy correction for the first order schemes. The rates of convergence are the same as above for all schemes, except for the energy relaxation method. Indeed, the first order approximation provides higher rates of convergence than in the Sod shock tube case. We may suggest that this important slope is due to the non-entropic shock which is vanishing. Thus the L^1 error would be mainly located close to the sonic point.

We may assume that this convergence is mainly led by the vanishing of the non-entropic shock computed by the VFRoe ncv (τ, u, p), and following the refinment could provide a rate of convergence similar to others VFRoe ncv schemes.

Case 2.3 Perfect gas EOS - Double subsonic rarefaction wave

This concerns Case 1.3, except for the fact that the initial velocity is set to : $u_L = -300$. As a result, the double rarefaction wave is subsonic (hence, the VFFC scheme provides meaningful results). Though the solution of this test case is continous, conections between waves and intermediate states are not regular. Thus, rates of convergence equals to 1 for the "first" order schemes and equals to 2 for the "second" order schemes cannot be expected. On the other hand, the contact discontinuity is a "ghost wave" (no variable jumps through this wave). This explains why the rate of convergence of the first order schemes is slightly higher for density than in previous cases. The rates of convergence of second order schemes are very close to 1. Note that the error associated with the Rusanov scheme is close to the error of other schemes.

Case 2.4 Perfect gas EOS - Double subsonic shock wave

The initial conditions of this test case come from the Case 1.4. Above mentionned remark concerning the contact discontinuity holds. For all schemes, the rates of convergence are slightly higher with the first order approximation than with the second order approximation (though the error of the first order schemes is more important). It can be explained by the occurence of oscillations on the intermediate state caused by the second order schemes.

3.3 Tammann EOS

As mentionned in section 1.5.2, one may retrieve by a suitable change of variables the Euler equations with perfect gas EOS from the Euler equations with Tammann EOS. Hence, the vacuum with the Tamman EOS is $\rho = 0$ and $p + p_c = 0$ and the condition for vacuum occurence (5) becomes :

$$\Delta u < \frac{2}{\gamma_c - 1}(c_L + c_R)$$

where $c^2 = \dfrac{\gamma_c(p + p_c)}{\rho}$.
However, this equivalence is only meaningful in the "continous" framework. Indeed, it no longer holds from a discrete point of view (except for PVRS and VFRoe ncv (τ, u, p)), and numerical results computed with the Tammann EOS are slightly different of previous results, namely with the perfect gas state law.

Case 3.1 Tammann EOS - Subsonic shock tube

This case is somewhat different from its counterpart with perfect gas EOS, and is based on initial conditions provided in [41]. However, the numerical approximation behaves as its counterpart with perfect gas EOS : all schemes provide good results, and Rusanov scheme is more diffusive than the others.

Left State	Right state
$\rho_L = 1100$	$\rho_R = 1000$
$u_L = 500$	$u_R = 0$
$p_L = 5.10^9$	$p_R = 10^5$

$$T_{MAX} = 0.6\, ms$$

Case 3.2 Tammann EOS - Sonic rarefaction wave

Once again, initial conditions are those provided in reference above. Note that the energy relaxation method (with the first order approximation) completely smears the non-entropic shock caused by VFRoe ncv (τ, u, p). All VFRoe ncv schemes have the same behaviour, and the Rusanov scheme is still more diffusive (first order or second order). Figures provided by first order schemes are presented (figures 1-6).

Left State	Right state
$\rho_L = 10^3$	$\rho_R = 10^3$
$u_L = 2000$	$u_R = 2000$
$p_L = 5.10^8$	$p_R = 10^6$

$$T_{MAX} = 8\ ms$$

Case 3.3 Tammann EOS - Double subsonic rarefaction wave

This test case is the counterpart of the Case 1.3. Note that vacuum (ie $\rho = 0$, $p + p_c = 0$) can occur within subsonic range, though it does not appear in this test case. Except for first order Rusanov scheme, all schemes compute a glitch (or a spike) at the interface (where the contact discontinuity is located) on the density.

Left State	Right state
$\rho_L = 10^3$	$\rho_R = 10^3$
$u_L = -300$	$u_R = 300$
$p_L = 10^9$	$p_R = 10^9$

$$T_{MAX} = 0,5\ ms$$

Case 3.4 Tammann EOS - Double subsonic shock wave

The only difference between this test case and the case presented above is due to the sign of initial velocities. As a result, in spite of rarefaction waves, the solution is composed by two shock waves and a ghost contact discontinuity. The same behaviour on the density can be noted, namely a glitch at the interface (even with the first order Rusanov scheme).

Left State	Right state
$\rho_L = 10^3$	$\rho_R = 10^3$
$u_L = 300$	$u_R = -300$
$p_L = 10^9$	$p_R = 10^9$

$$T_{MAX} = 0,5\ ms$$

Case 3.5 Tammann EOS - Stationary 1-shock wave

A very slight difference may be seen when the average value of $\hat{\gamma}$ is chosen as $0.5((\hat{\gamma})_L + (\hat{\gamma})_R)$ instead of $\tilde{\hat{\gamma}} = \hat{\gamma}(\overline{Y})$ when focusing on VFRoe ncv with variable (τ, u, p). The shock remains steady only if the the latter choice is considered from a theoretical point of view, which is confirmed by computation. However, other VFRoe ncv schemes provide as accurate results. First or second order Rusanov scheme is very diffusive, and the energy relaxation method introduces three or two points in the shock profile, according to the order of approximation.

Left State	Right state
$\rho_L = 2.10^{-10}$	$\rho_R = u_R^{-1}$
$u_L = 5.10^9$	$u_R = \frac{4\gamma_c}{\gamma_c+1} p_c + \frac{\gamma_c-1}{\gamma_c+1} 5.10^9$
$p_L = p_c$	$p_R = p_L + u_L - u_R$

$$T_{MAX} = 10^{-9}\ s$$

Case 3.6 Tammann EOS - Unsteady contact discontinuity

The results provided by all schemes are similar to those provided with the perfect gas EOS (see Case 1.6). Pressure and velocity are exactly preserved (see appendix A), and the jump of density is smeared by all schemes (in particular by the Rusanov scheme).

Left State	Right state
$\rho_L = 10^3$	$\rho_R = 10^2$
$u_L = 10^3$	$u_R = 10^3$
$p_L = 10^8$	$p_R = 10^8$

$$T_{MAX} = 2\ ms$$

Case 3.7 Tammann EOS - Rarefaction wave propagating over vacuum

This test computes a 1-rarefaction wave with a sonic point. The 2-contact discontinuity and the 3-shock wave are not of significant importance, like in the Case 1.7. We have used in the following last two cases : $\widetilde{\hat{\gamma}} = \hat{\gamma}(\overline{Y})$. In this case, only VFRoe ncv (τ, u, p) with RK2-MUSCL integration (figures 7-8) and (first or second order) Rusanov scheme enable computation (see figures 9-10 for the first order). Note that the standard choice $0.5((\hat{\gamma})_L + (\hat{\gamma})_R)$ results in a blow up of the computation. Initial conditions make all other schemes blow up. These behaviours confirm the discrete difference between perfect gas EOS and Tammann EOS.

Left State	Right state
$\rho_L = 10^3$	$\rho_R = 10^{-9}$
$u_L = 0$	$u_R = 0$
$p_L = 10^8$	$p_R + p_c = 10^{-2}$

$$T_{MAX} = 0,6\ ms$$

Case 3.8 Tammann EOS - Vacuum occurence

This test results like Case 1.8 in a vacuum occurence in the intermediate state. Recall that vacuum can appear though rarefaction waves are not supersonic. As above, VFRoe ncv (τ, u, p) and Rusanov schemes enable computation. Note that PVRS and VFRoe schemes also perform well in this test (see figures 11-14).

Left State	Right state
$\rho_L = 10^3$	$\rho_R = 10^3$
$u_L = 1500$	$u_R = 1500$
$p_L = 10^9$	$p_R = 10^9$

$$T_{MAX} = 0,6\ ms$$

3.4 Van Der Waals EOS

Results of both computations discussed below were achieved using the standard definition for VFRoe ncv (τ, u, p) and PVRS schemes of the mean of $\hat{\gamma}$: $0.5((\hat{\gamma})_L + (\hat{\gamma})_R)$ instead of : $\widetilde{\hat{\gamma}} = \hat{\gamma}(\overline{Y})$ when focusing on VFRoe ncv scheme. Differences between results for both choices could hardly be noticed for the following.

Case 4.1 Van Der Waals EOS - Subsonic 1-rarefaction wave

Initial conditions below are taken from the paper by Letellier and Forestier [30]. The main advantage of this case is that it clearly exhibits the rather unpleasant behaviour around the contact discontinuity. Though both the exact Godunov scheme and VFRoe scheme with (τ, u, p) variables predict equal velocity and pressure of intermediate states on each side of the LD field, cell values of both u and p are not in equilibrium (this confirms results of appendix A for the VFRoe schemes with (φ, u, p) variable). Obviously this well-known drawback (see [30]) tends to vanish when the mesh size decreases, or when time increases. First order results are provided on figures 15-20.

Left State	Right state
$\rho_L = 333,33$	$\rho_R = 111,11$
$u_L = 0$	$u_R = 0$
$p_L = 37311358$	$p_R = 21770768$

$$T_{MAX} = 5\ ms$$

Case 4.2 Van Der Waals EOS - Moving contact discontinuity

Initial conditions are similar to those given in Case 1.6. Note that the Riemann invariants u and p are not very well preserved around the contact discontinuity when using coarse meshes, and "first" order scheme (see appendix A for more details on VFRoe ncv schemes with (φ, u, p) variable). The "second' order version of the scheme performs much better. Unlike sometimes heard, we emphasize that the approximation is still convergent. Small oscillations apart from the LD scheme which were reported in [30] do not arise when using approximate Godunov schemes, which is still unexplained and rather amazing. Due to the very small rate of convergence measured in the LD field (smaller than 2/3) , it is clear that this slows down the whole rate of convergence on both velocity and

pressure variable, compared with what happens when focusing on perfect gas EOS. Hence, none among schemes presented here are able to preserve velocity and pressure constant on a given mesh (see figures 21-26 for results performed by first order schemes).

Left State	Right state
$\rho_L = 1$	$\rho_R = 10$
$u_L = 100$	$u_R = 100$
$p_L = 10^5$	$p_R = 10^5$

$T_{MAX} = 6\ ms$

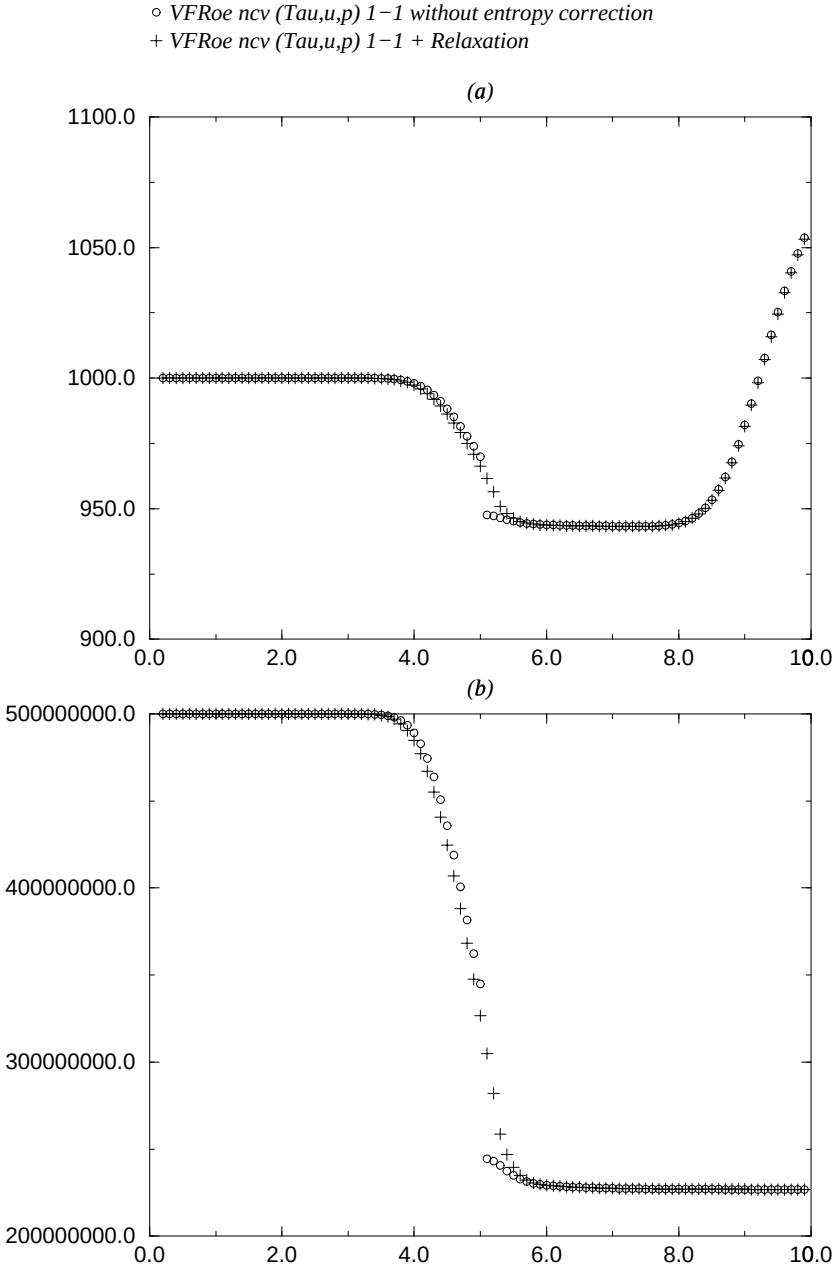

Figure 1: Case 3.2 : density (a) - $p + p_c$ (b)

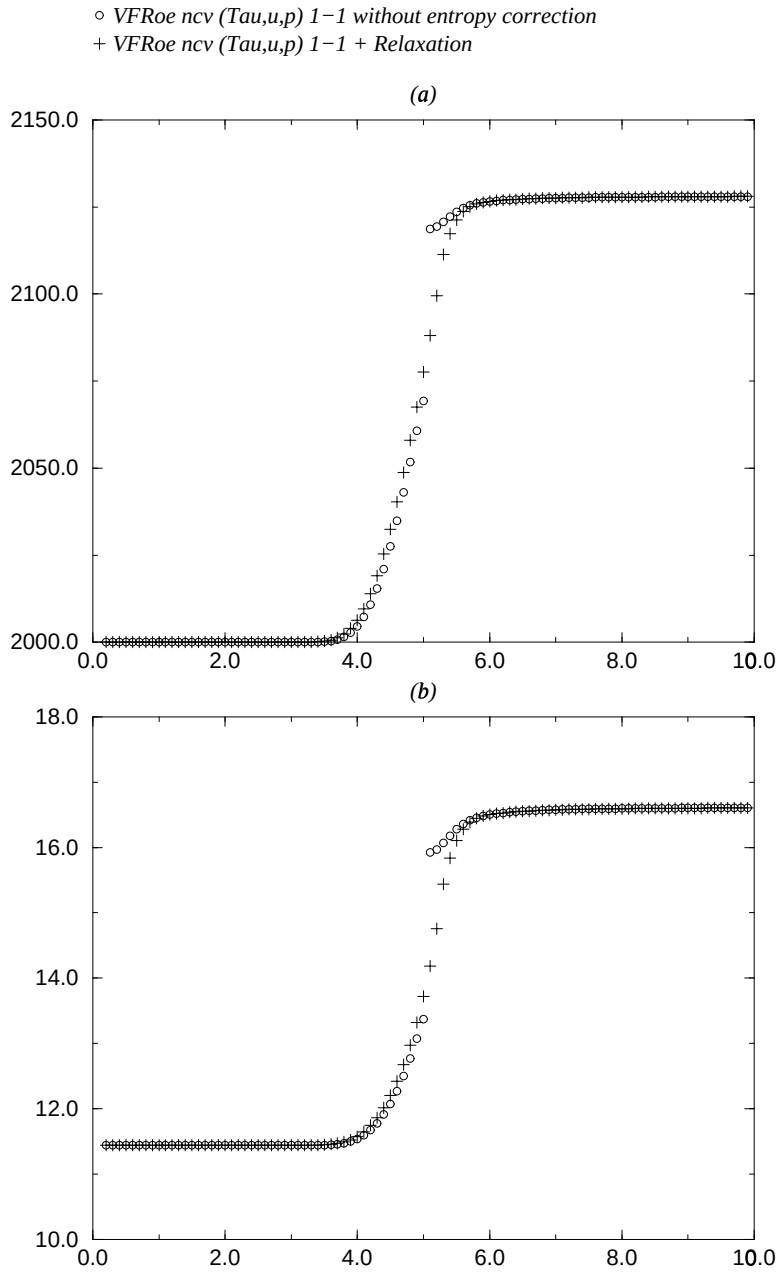

Figure 2: Case 3.2 : velocity (a) - $\hat{\gamma}(p,\rho)$ (b)

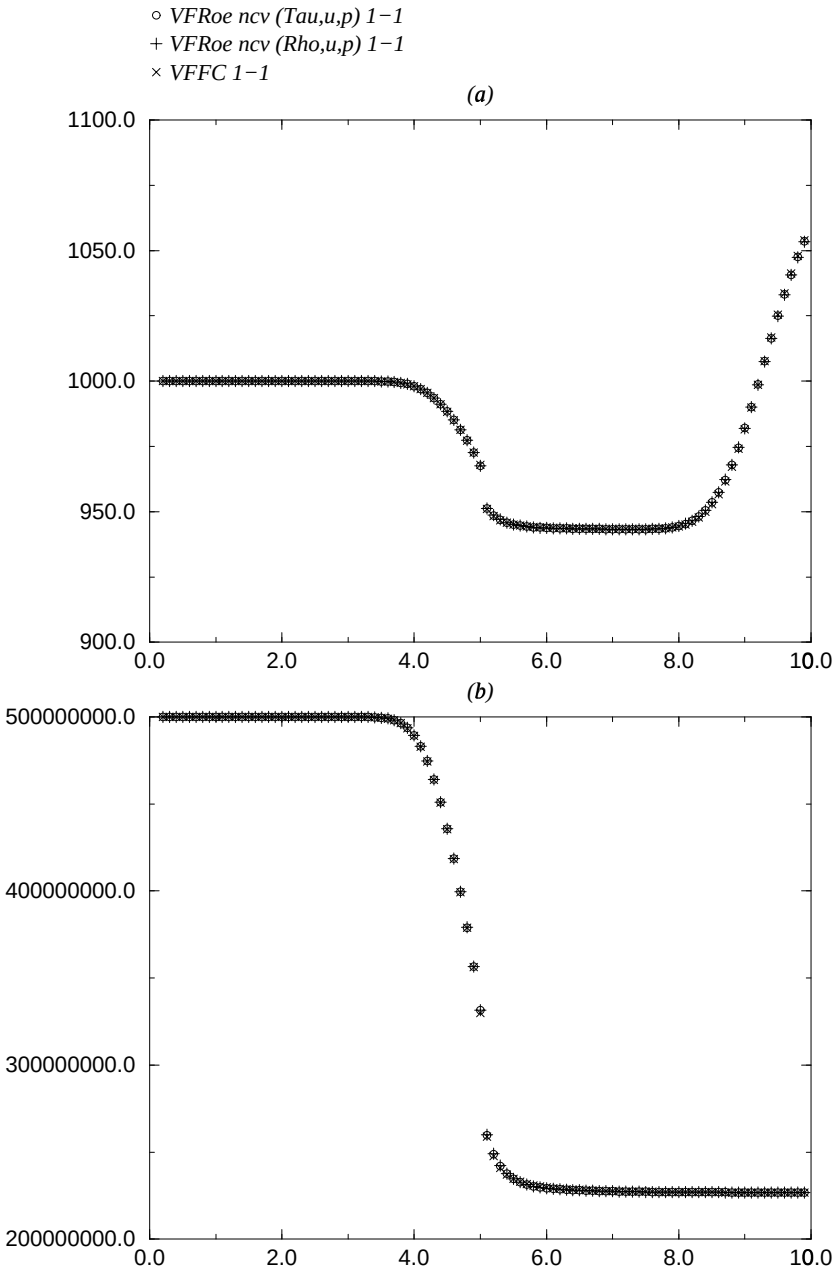

Figure 3: Case 3.2 : density (a) - $p + p_c$ (b)

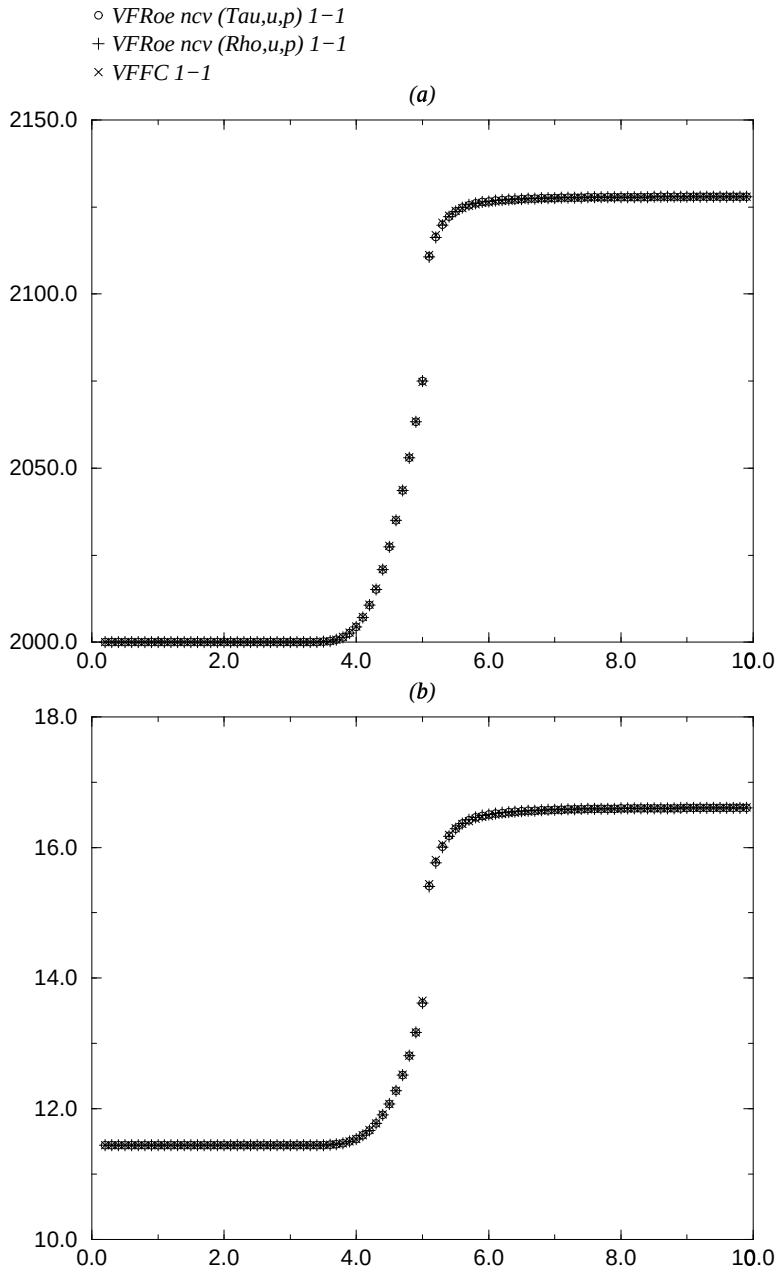

Figure 4: Case 3.2 : velocity (a) - $\hat{\gamma}(p,\rho)$ (b)

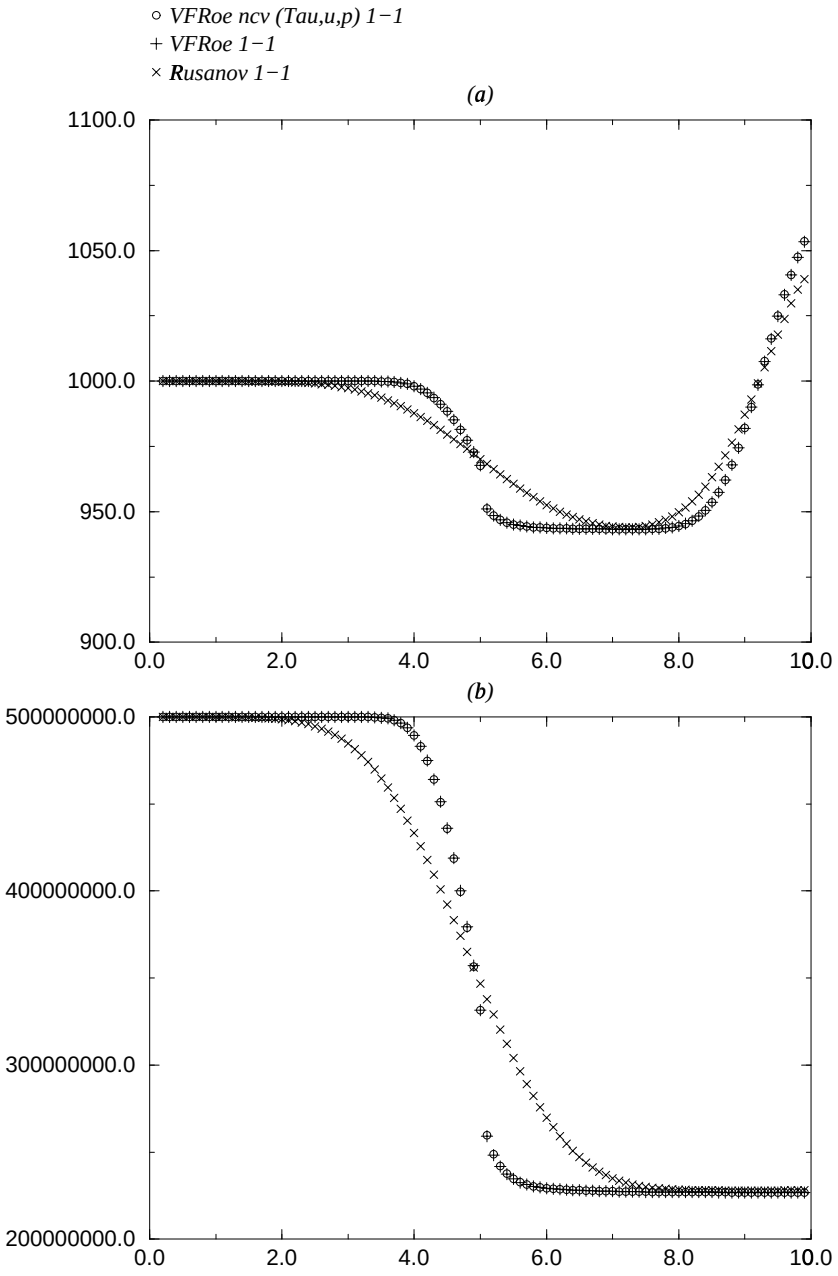

Figure 5: Case 3.2 : density (a) - $p + p_c$ (b)

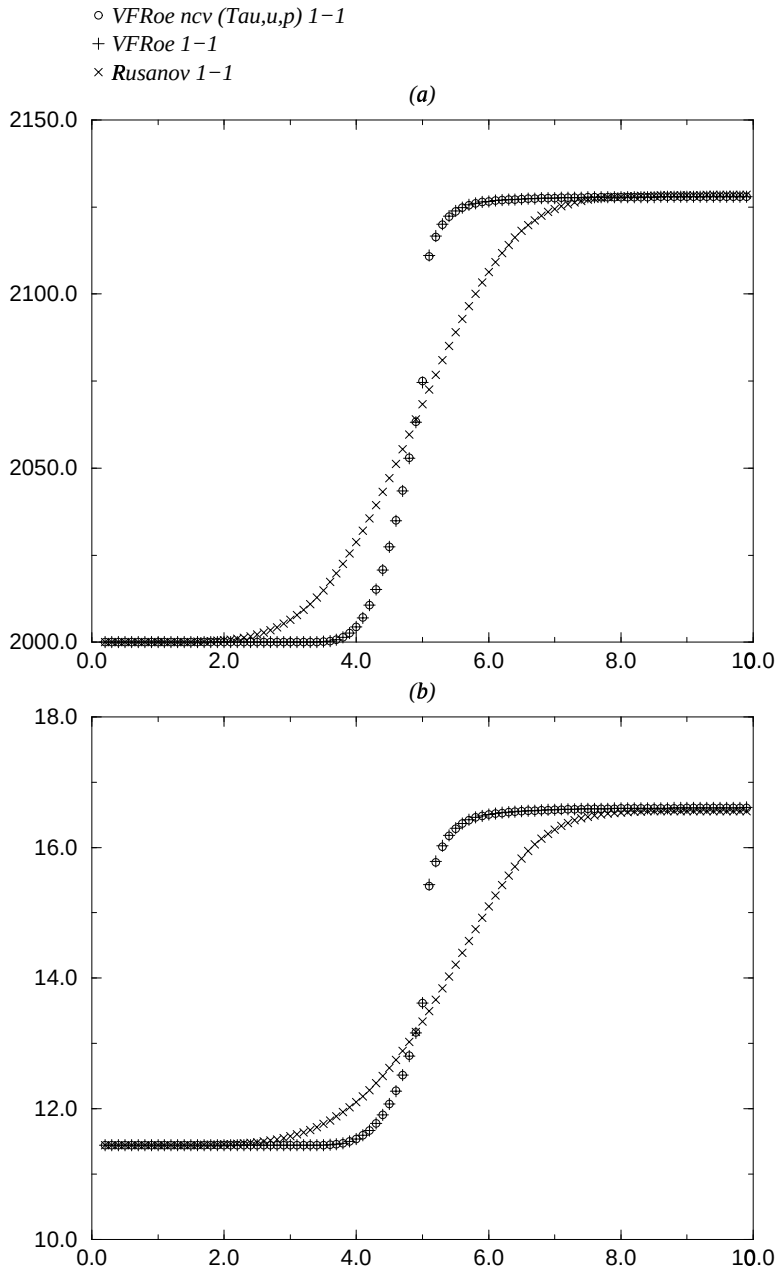

Figure 6: Case 3.2 : velocity (a) - $\hat{\gamma}(p,\rho)$ (b)

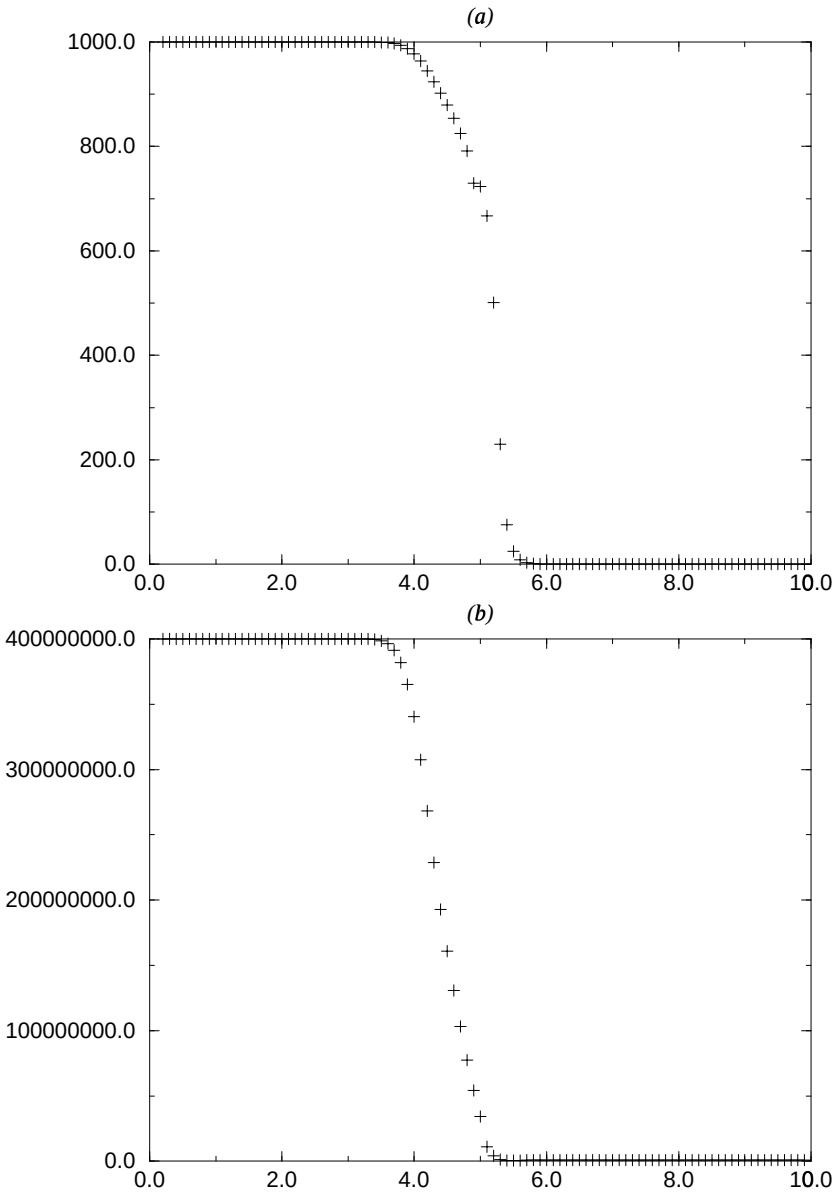

Figure 7: Case 3.7 : densité (a) - $p + p_c$ (b)

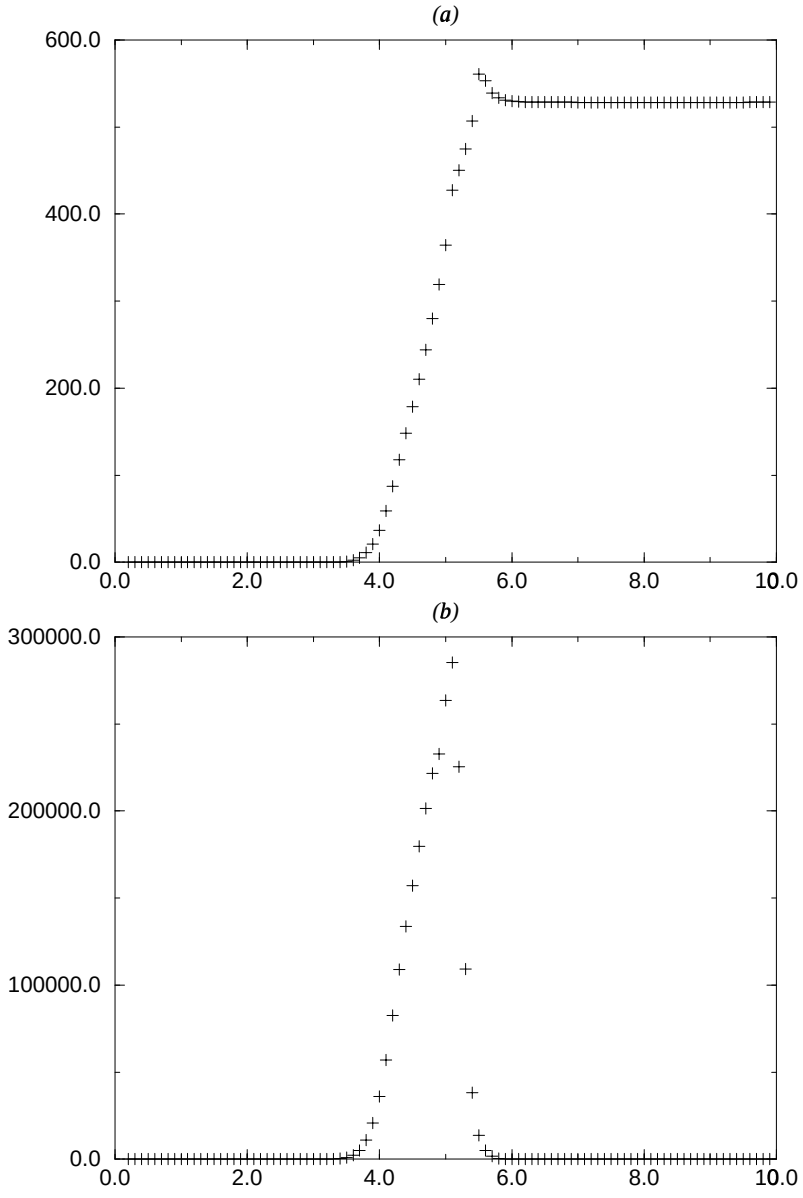

Figure 8: Case 3.7 : vitesse (a) - momentum (b)

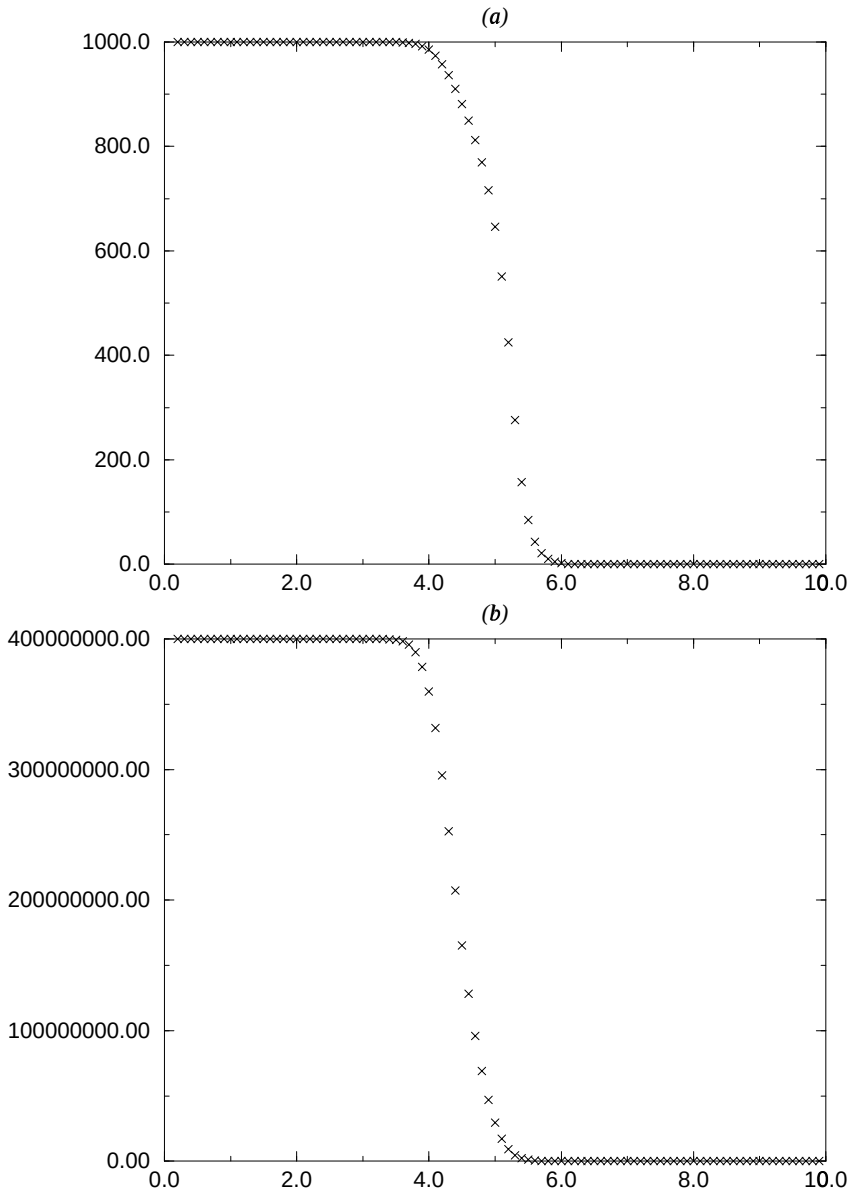

Figure 9: Case 3.7 : density (a) - $p + p_c$ (b)

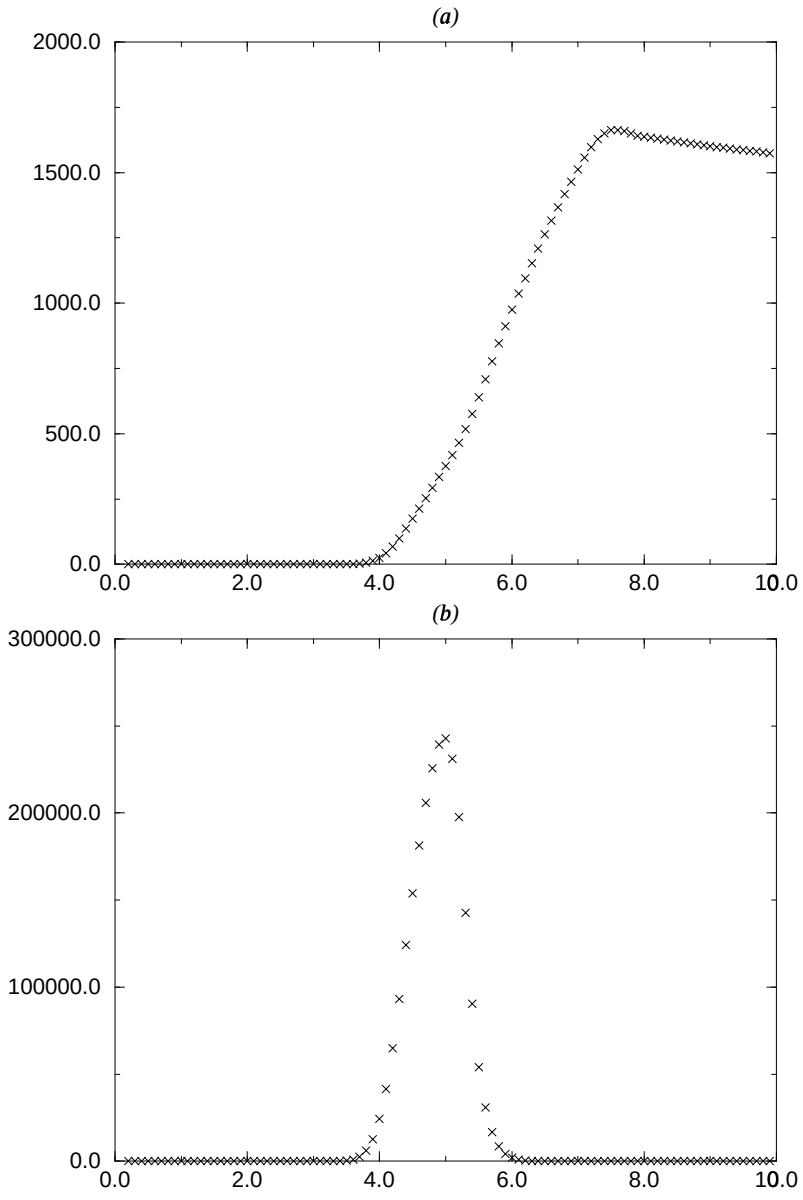

Figure 10: Case 3.7 : velocity (a) - momentum (b)

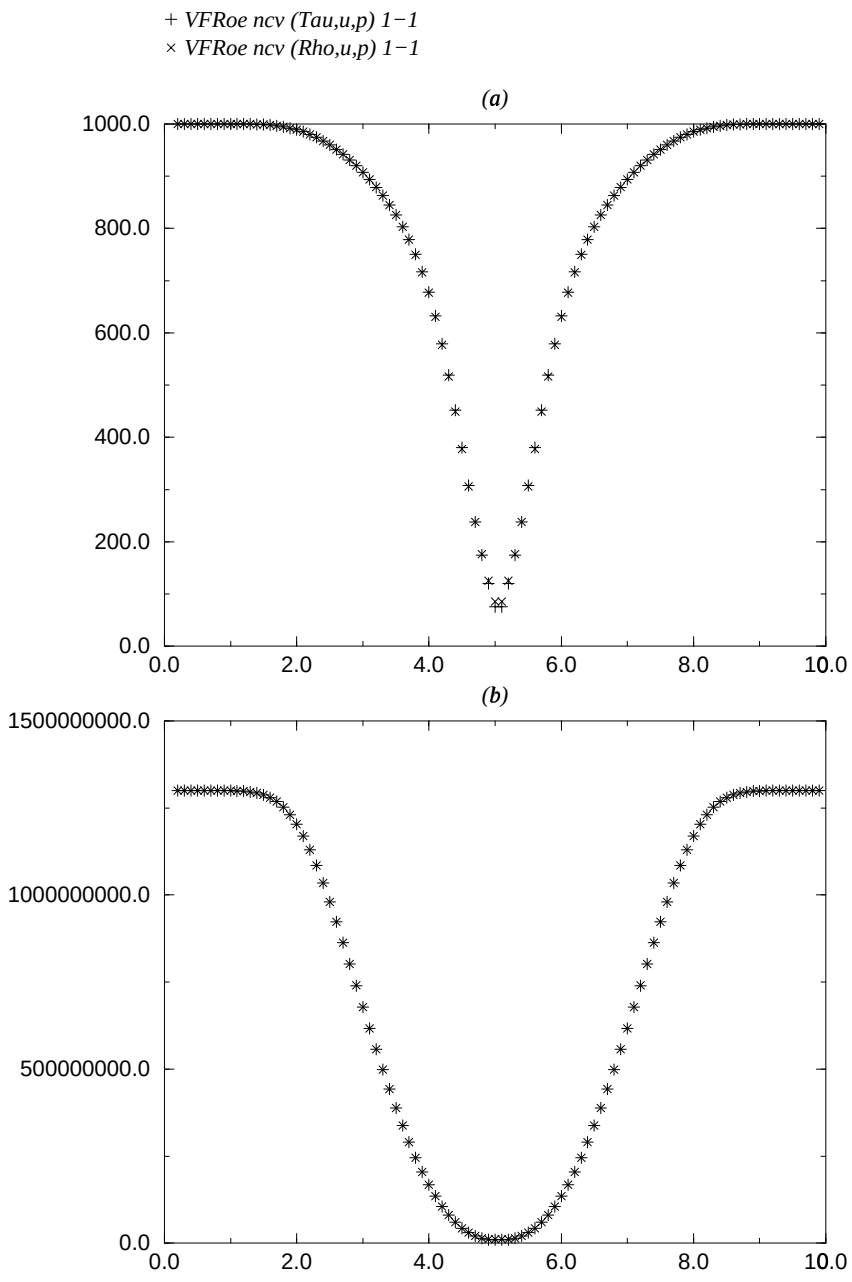

Figure 11: Case 3.8 : densité (a) - $p + p_c$ (b)

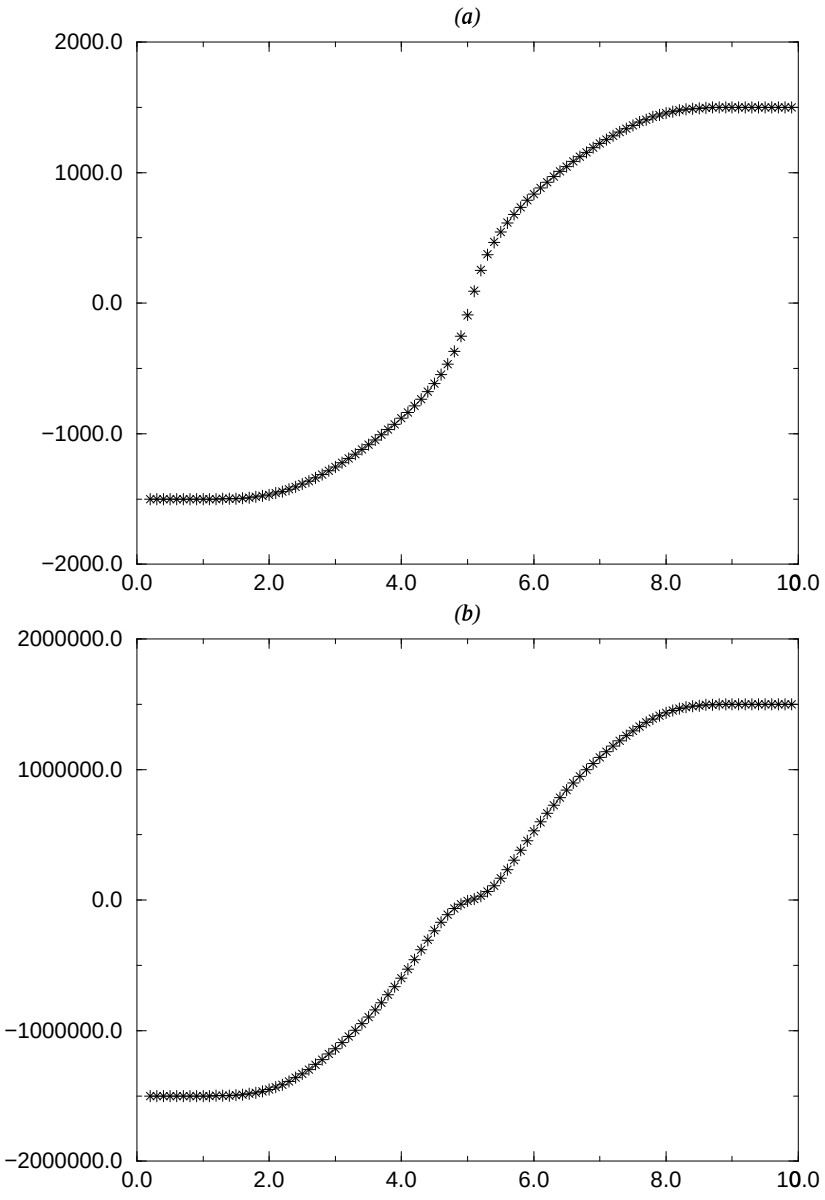

Figure 12: Case 3.8 : vitesse (a) - momentum (b)

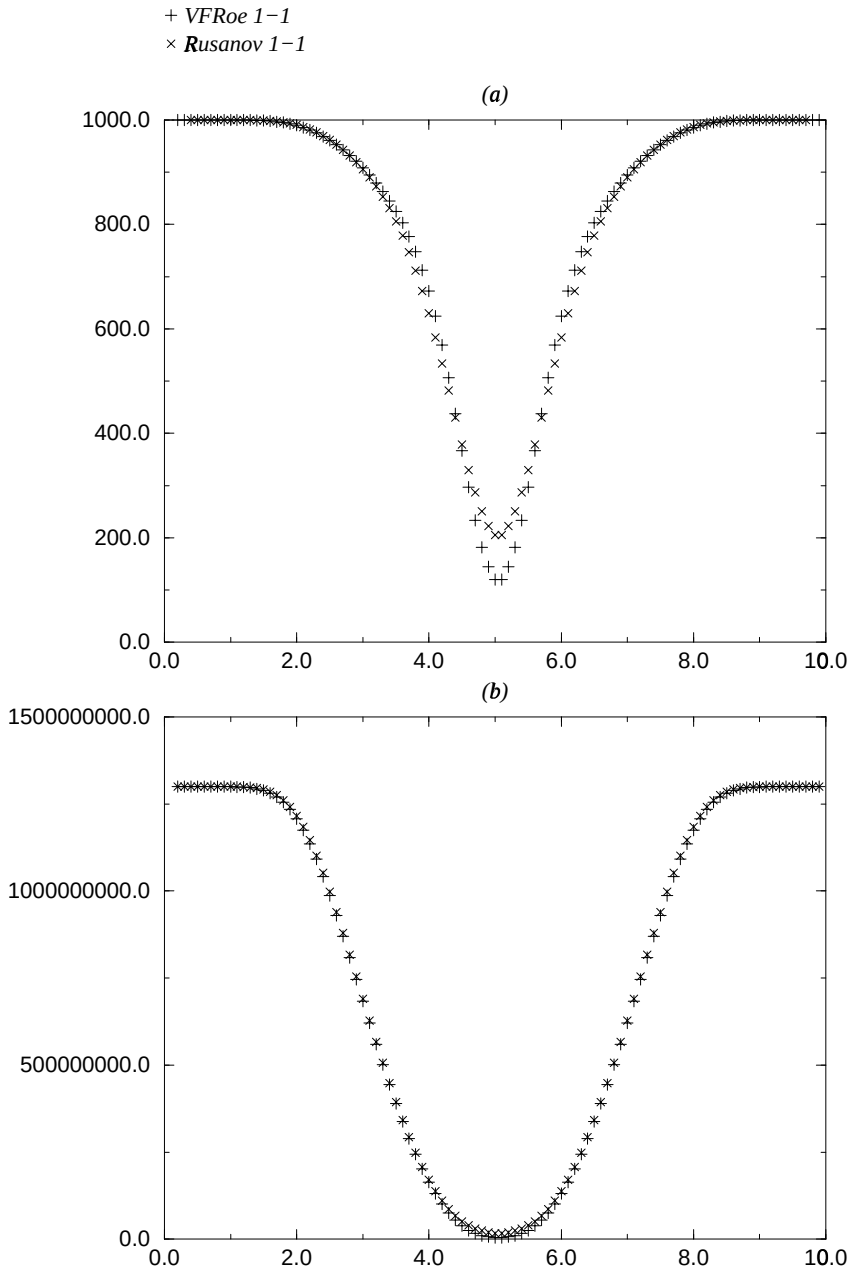

Figure 13: Case 3.8 : density (a) - $p + p_c$ (b)

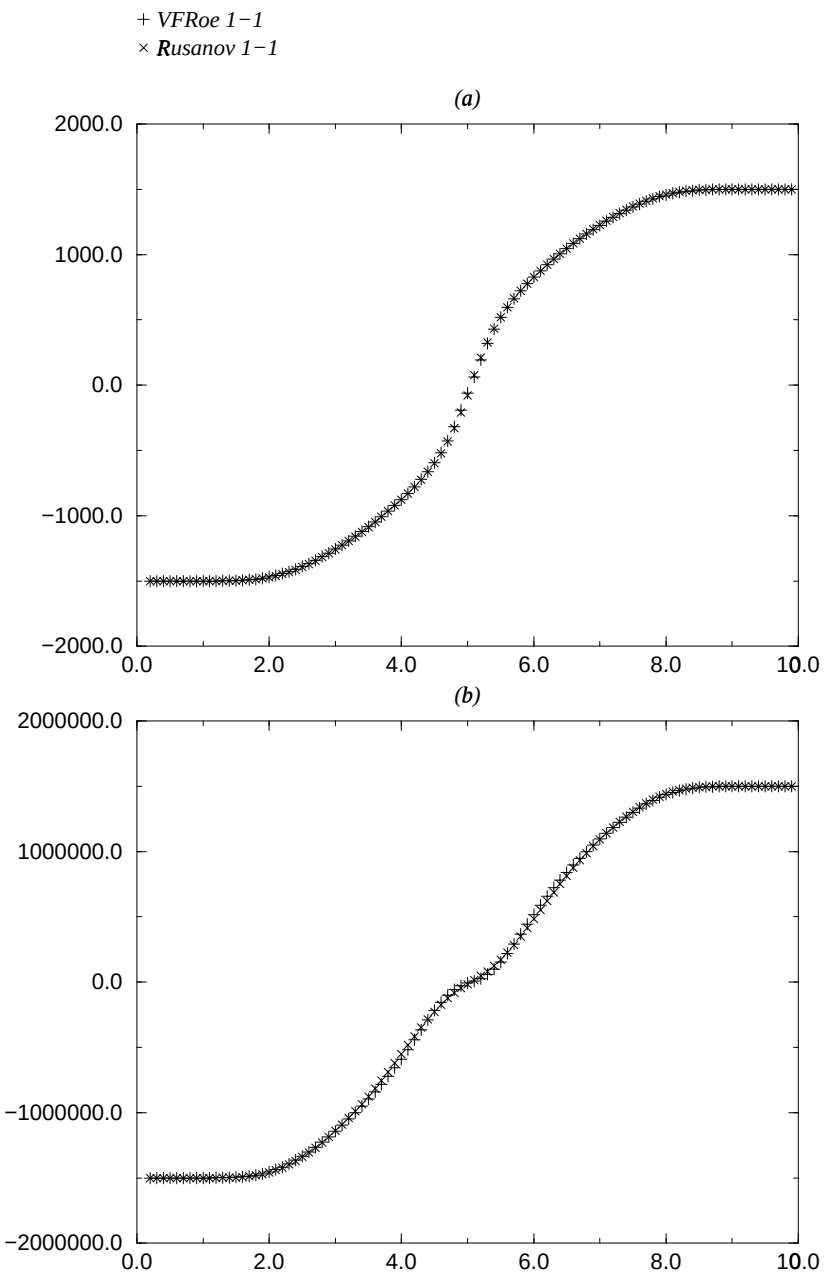

Figure 14: Case 3.8 : velocity (a) - momentum (b)

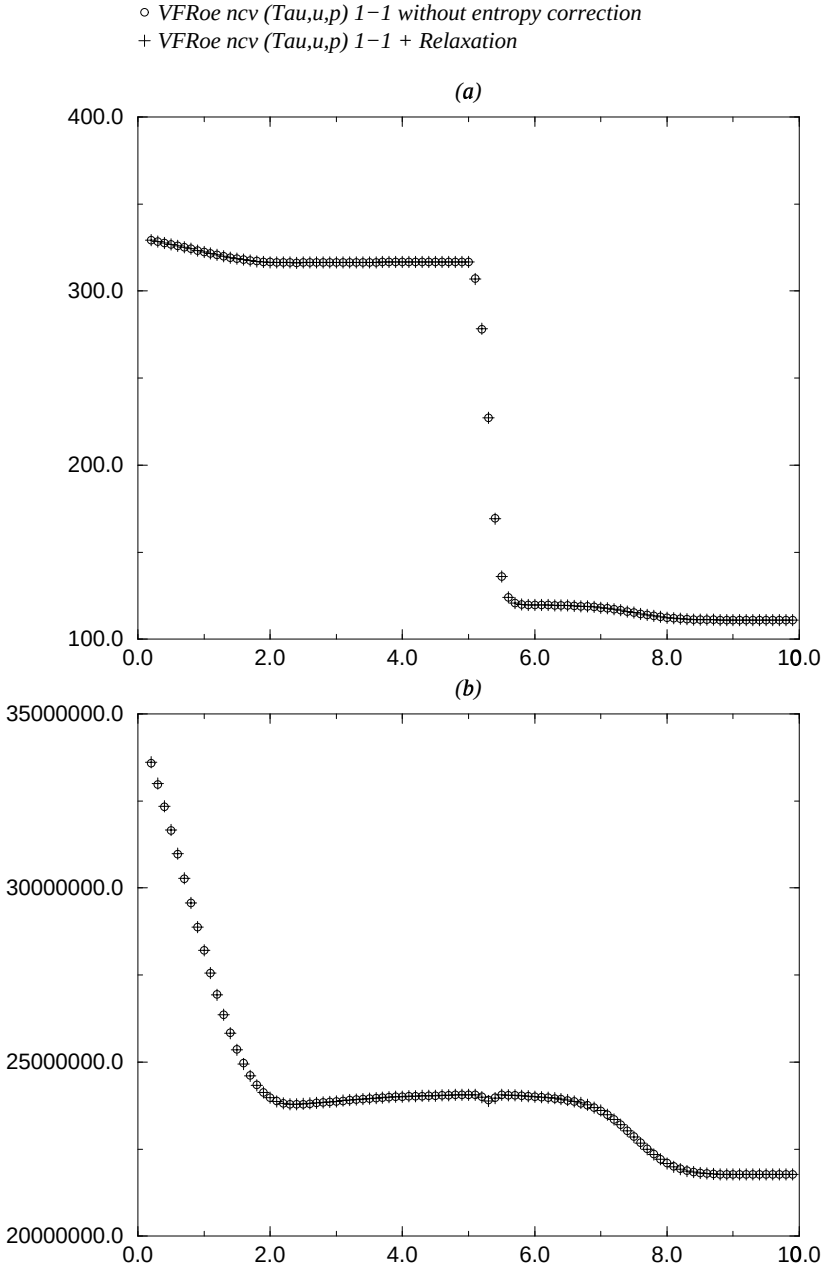

Figure 15: Case 4.1 : densité (a) - $p + p_c$ (b)

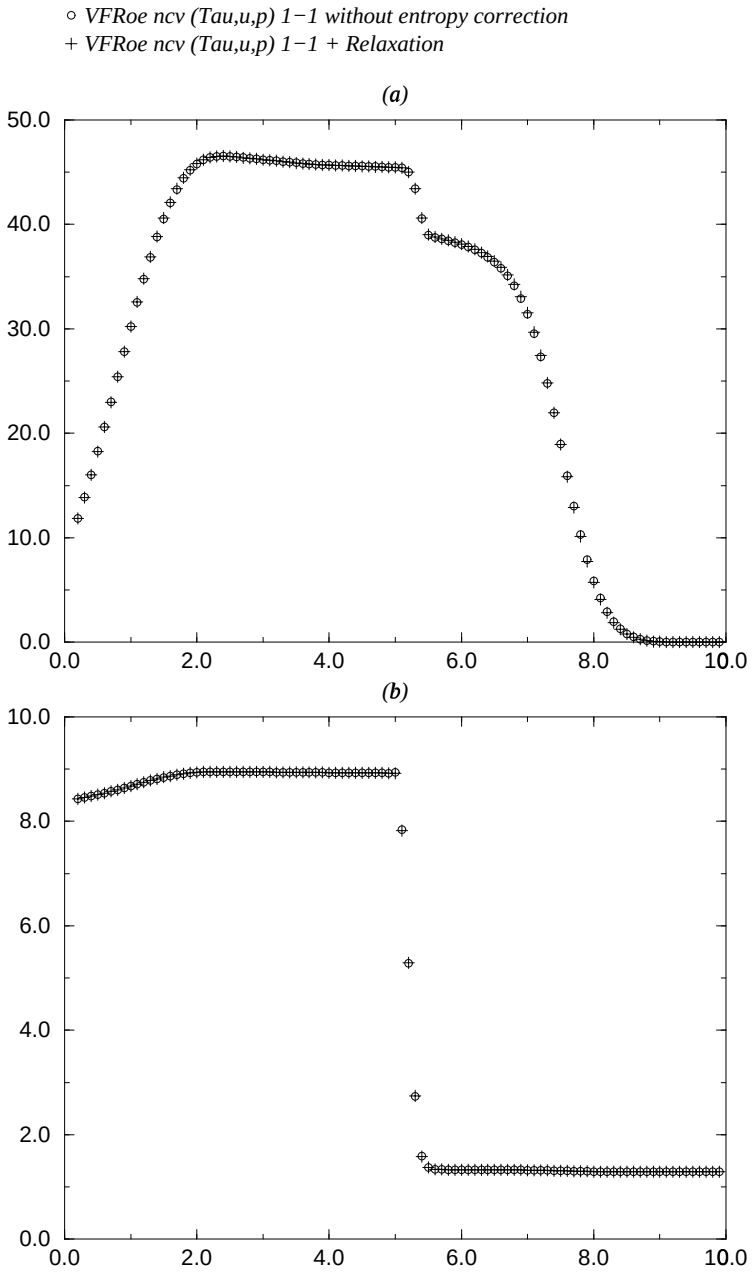

Figure 16: Case 4.1 : vitesse (a) - $\hat{\gamma}(p,\rho)$ (b)

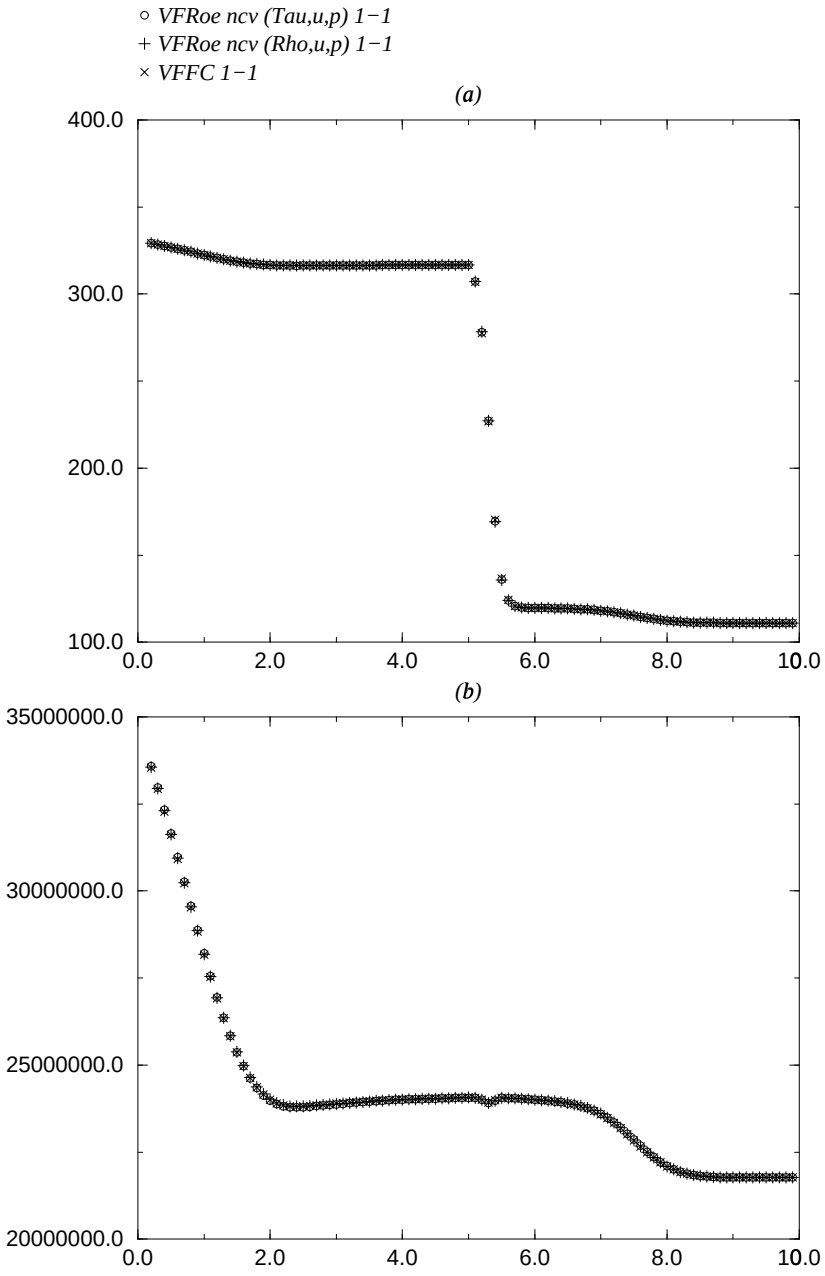

Figure 17: Case 4.1 : densité (a) - $p + p_c$ (b)

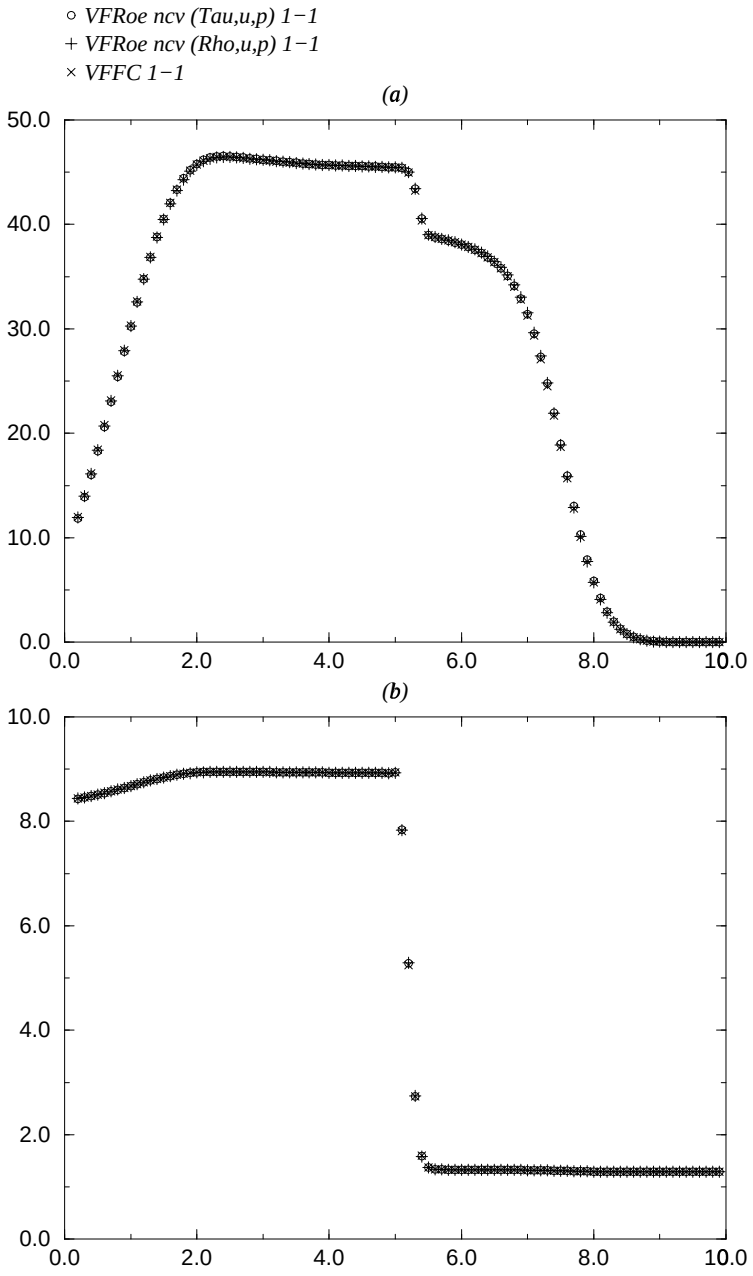

Figure 18: Case 4.1 : vitesse (a) - $\hat{\gamma}(p,\rho)$ (b)

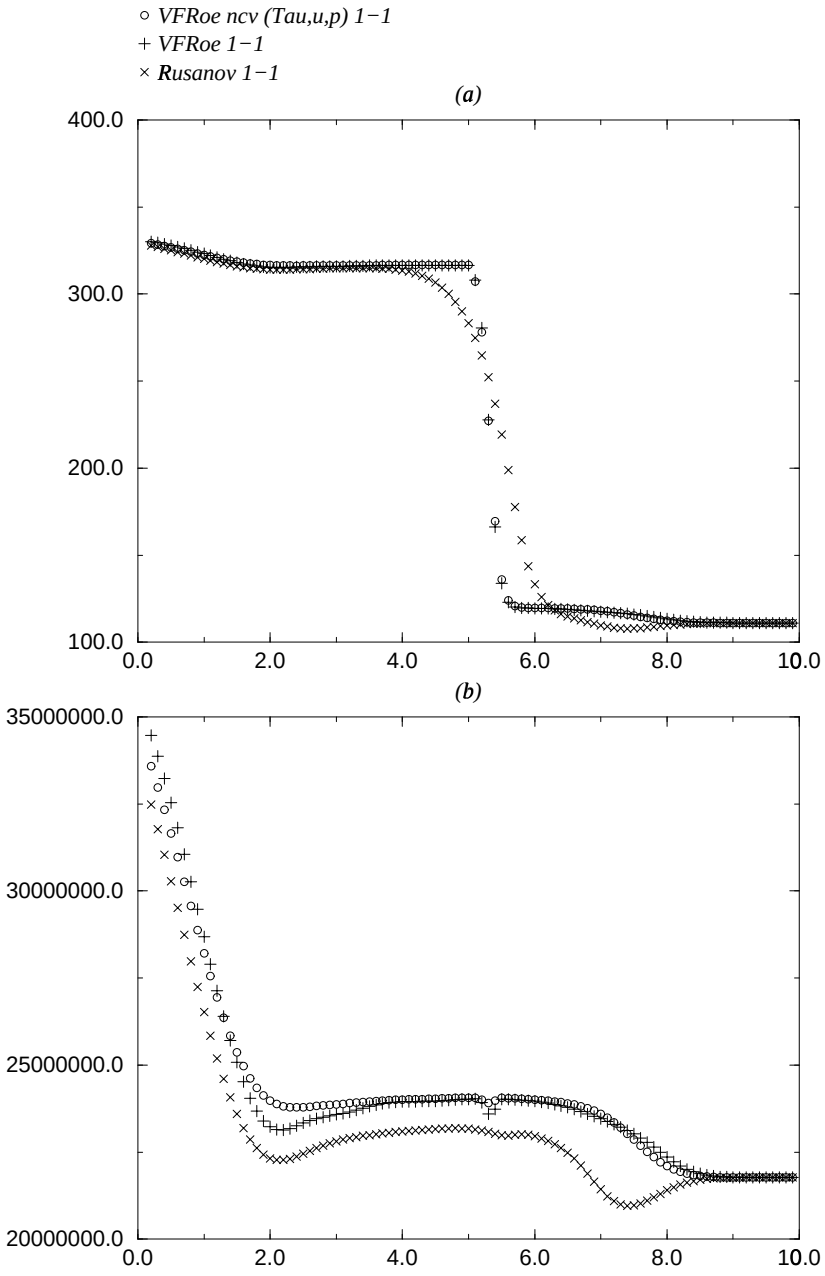

Figure 19: Case 4.1 : densité (a) - $p + p_c$ (b)

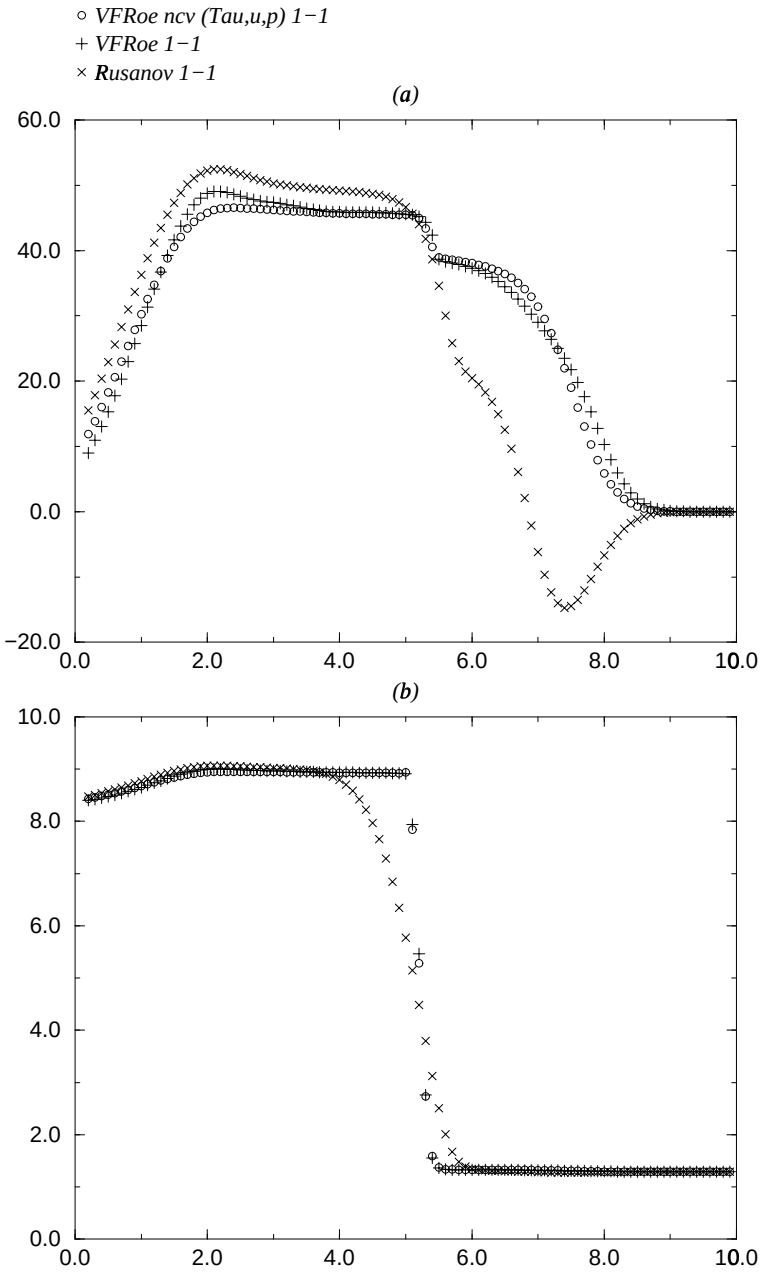

Figure 20: Case 4.1 : vitesse (a) - $\hat{\gamma}(p,\rho)$ (b)

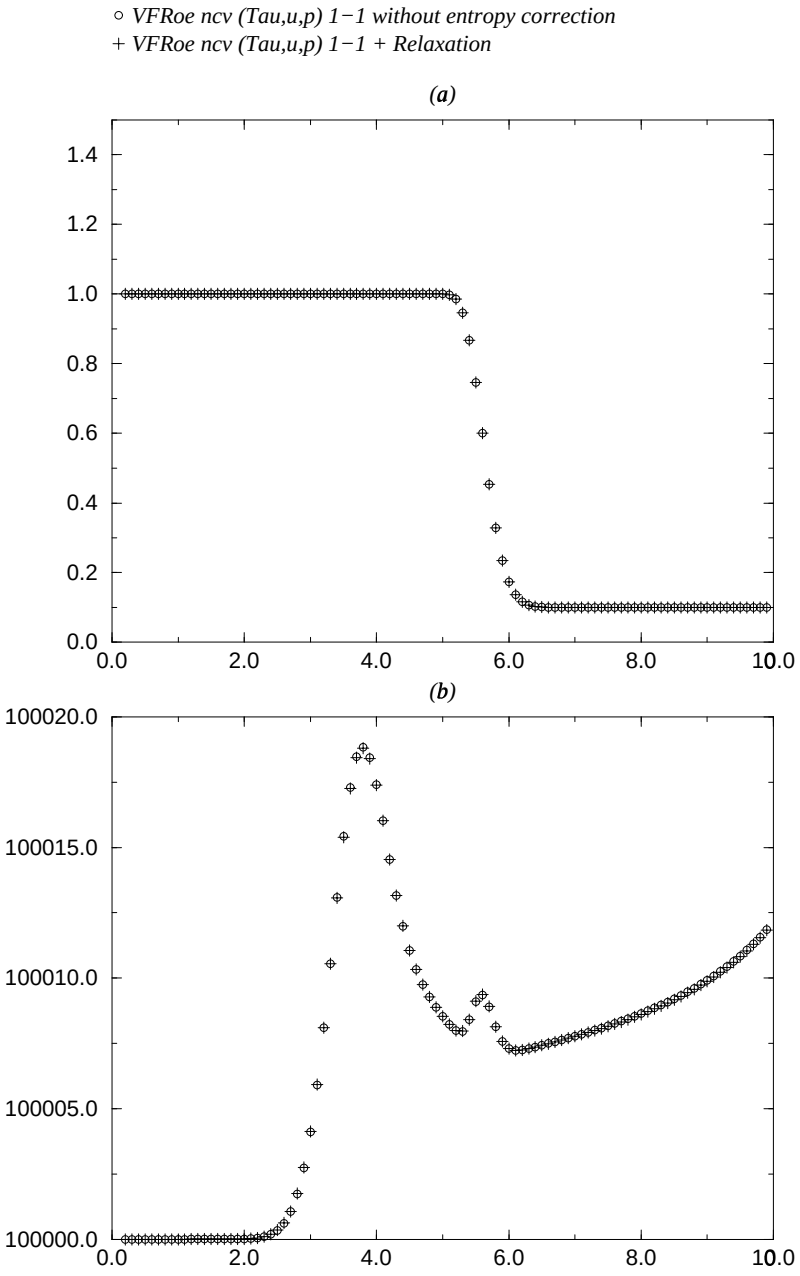

Figure 21: Case 4.2 : densité (a) - $p + p_c$ (b)

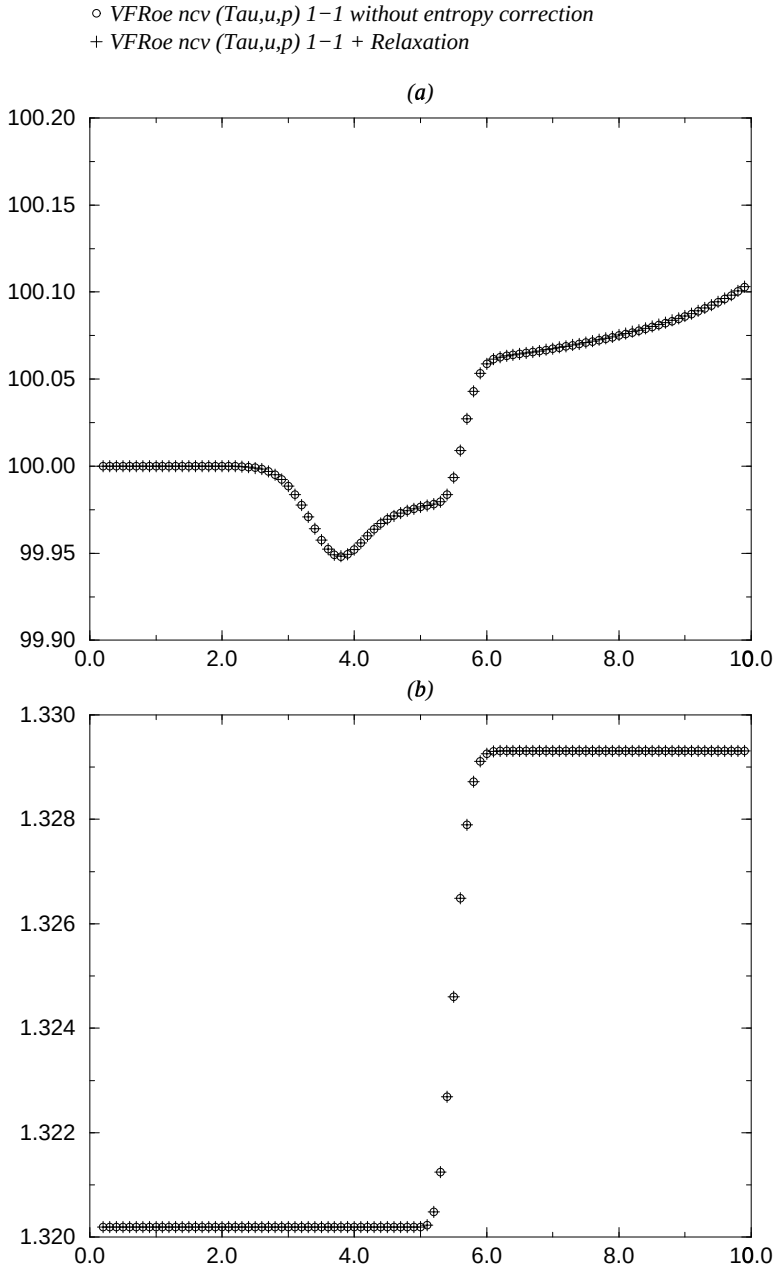

Figure 22: Case 4.2 : vitesse (a) - $\hat{\gamma}(p,\rho)$ (b)

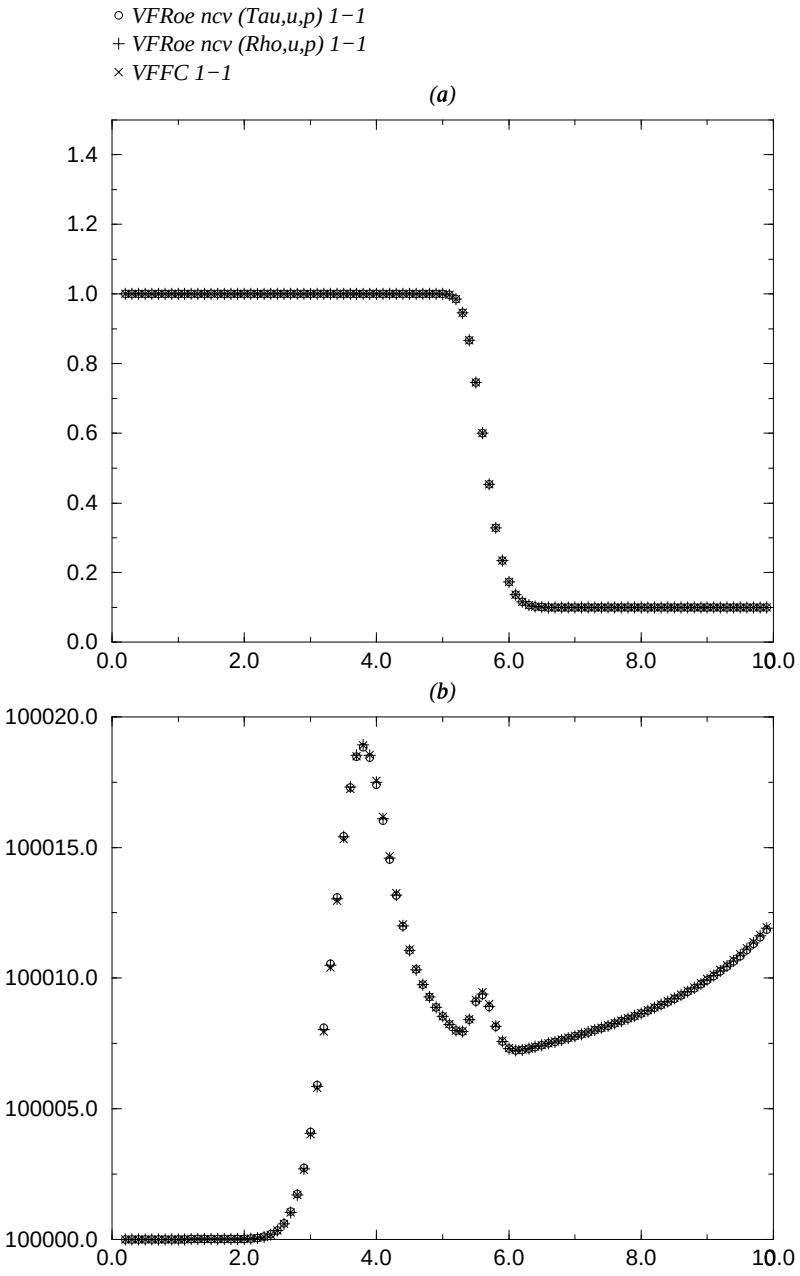

Figure 23: Case 4.2 : densité (a) - $p + p_c$ (b)

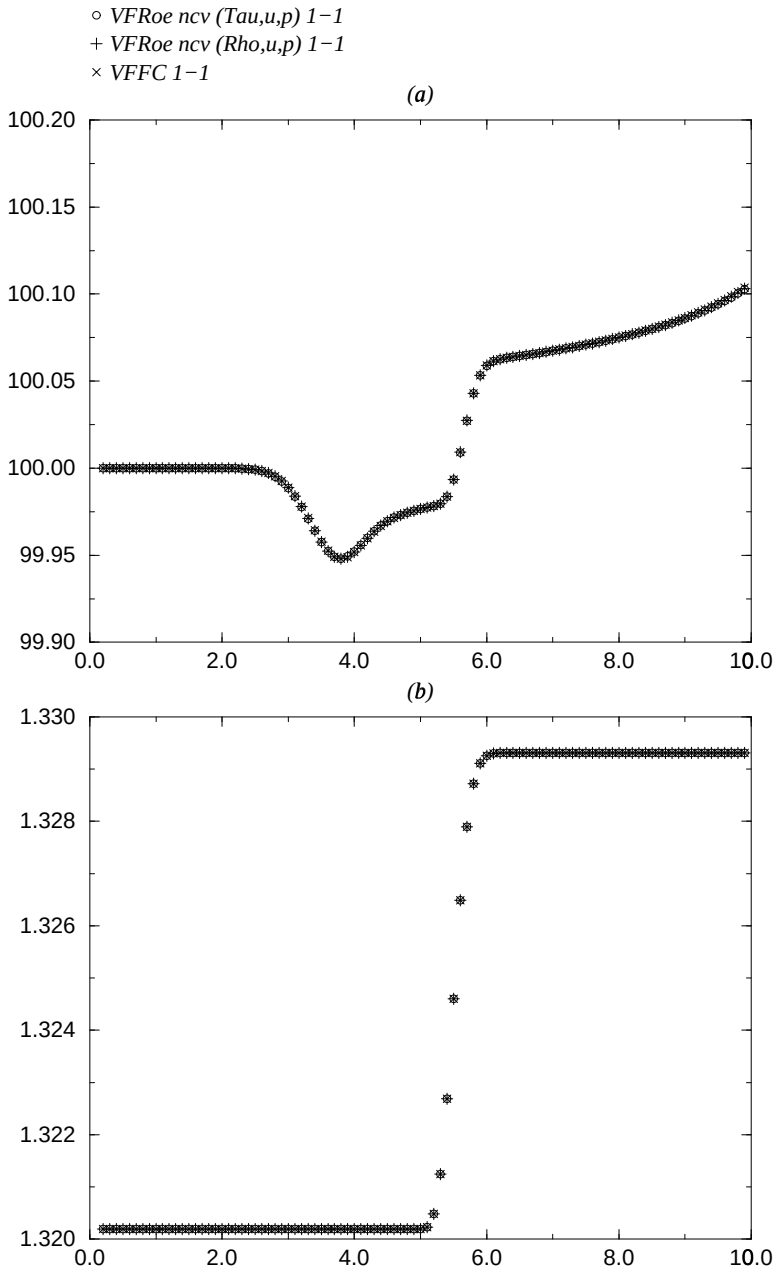

Figure 24: Case 4.2 : vitesse (a) - $\hat{\gamma}(p,\rho)$ (b)

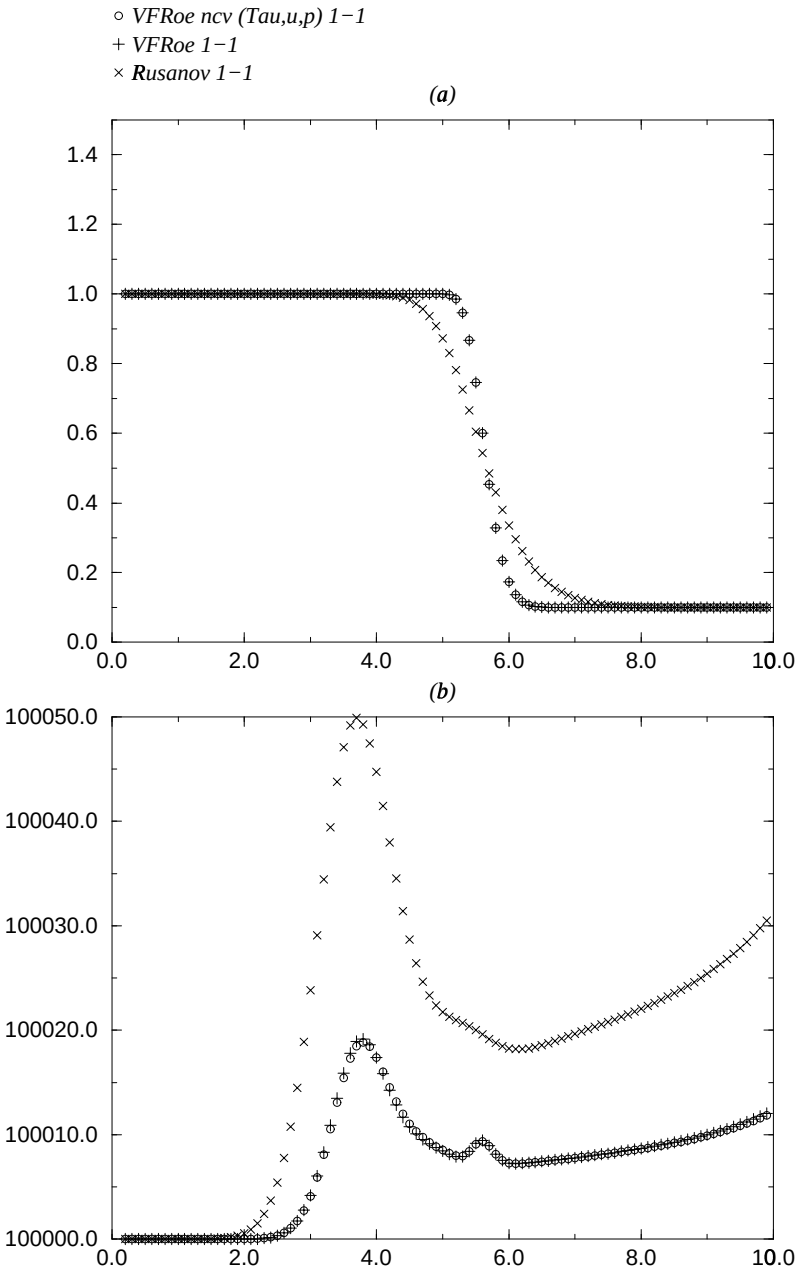

Figure 25: Case 4.2 : densité (a) - $p + p_c$ (b)

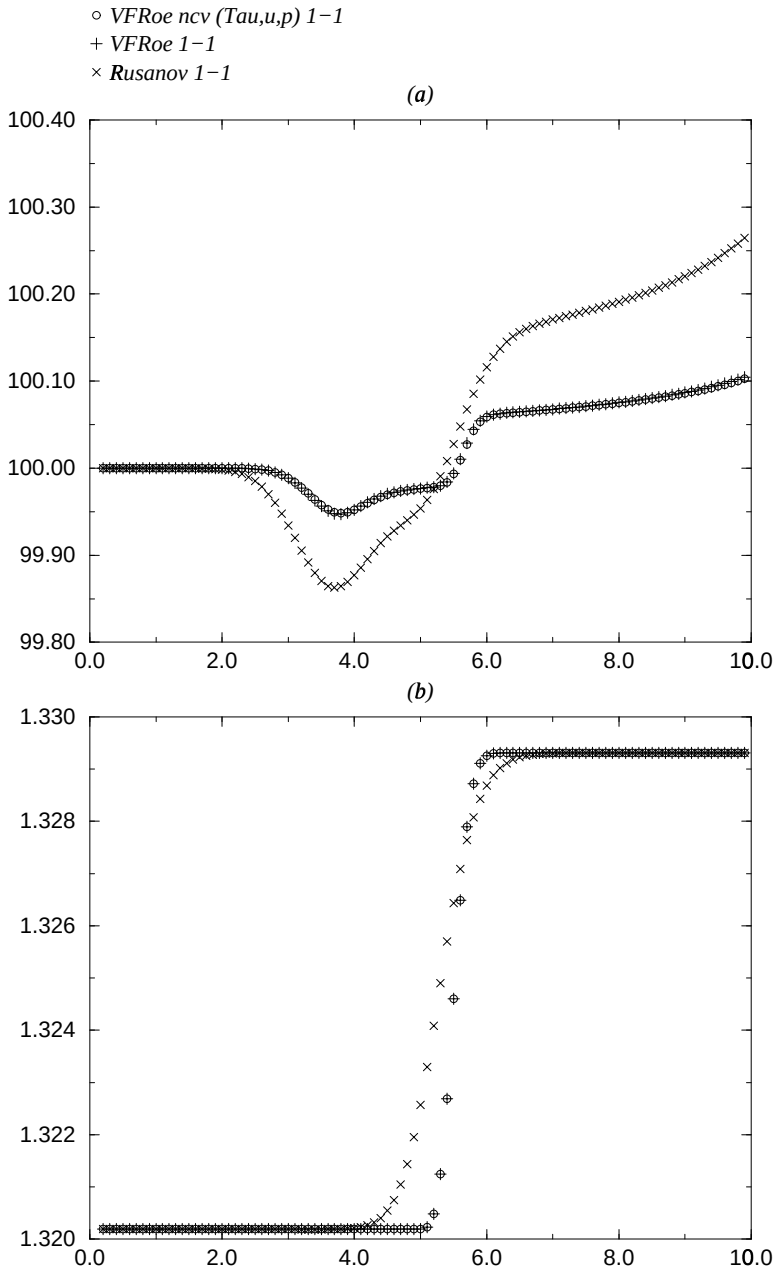

Figure 26: Case 4.2 : vitesse (a) - $\hat{\gamma}(p,\rho)$ (b)

3.5 Actual rates of convergence

Perfect gas EOS - Sod shock tube

- Energy relaxation

	1st order	2nd order
ρ	0.654	0.791
u	0.853	0.967
p	0.812	0.988

- Rusanov

	1st order	2nd order
ρ	0.651	0.780
u	0.842	0.970
p	0.823	0.989

- VFFC

	1st order	2nd order
ρ	0.655	0.792
u	0.855	0.968
p	0.814	0.988

- VFRoe

	1st order	2nd order
ρ	0.654	0.791
u	0.853	0.967
p	0.811	0.988

- VFRoe ncv (ρ, u, p)

	1st order	2nd order
ρ	0.654	0.791
u	0.853	0.967
p	0.811	0.988

- VFRoe ncv (τ, u, p)

	1st order	2nd order
ρ	0.653	0.791
u	0.853	0.967
p	0.812	0.988

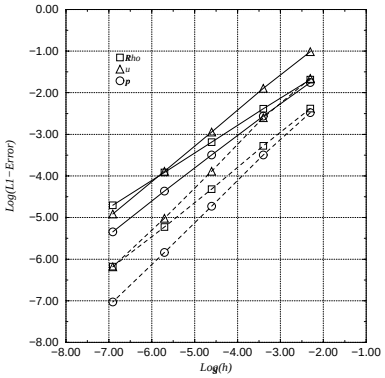

Figure 27: Relaxation d'énergie

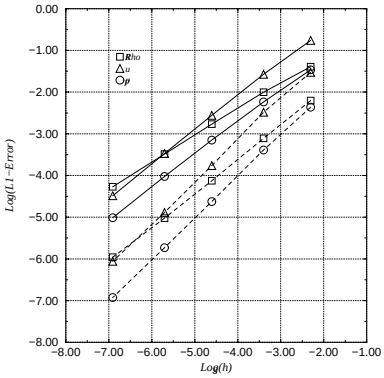

Figure 28: Rusanov

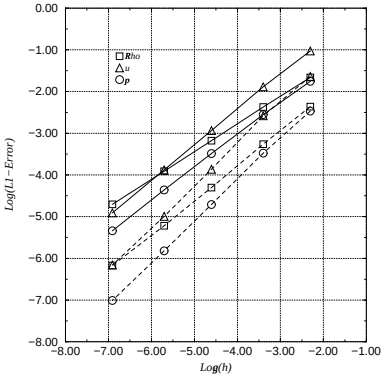

Figure 29: VFFC

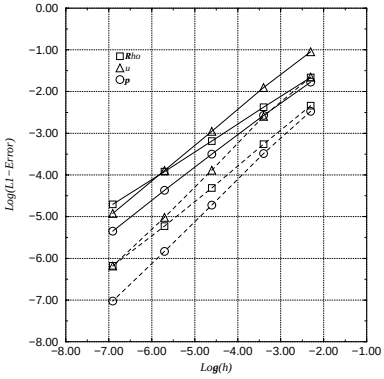

Figure 30: VFRoe

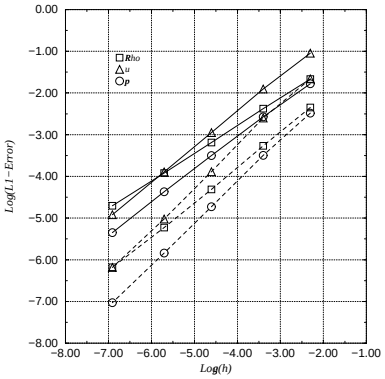

Figure 31: VFRoe ncv (ρ, u, p)

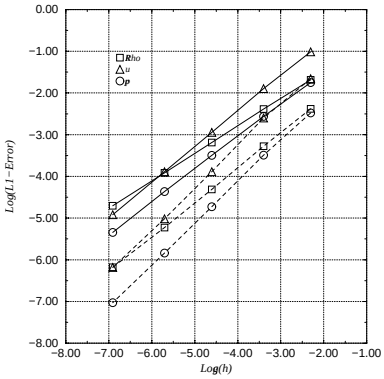

Figure 32: VFRoe ncv (τ, u, p)

Perfect gas EOS - Sonic rarefaction wave

- Energy relaxation

	1st order	2nd order
ρ	0.890	0.810
u	0.933	0.973
p	0.927	0.995

- Rusanov

	1st order	2nd order
ρ	0.684	0.827
u	0.794	0.985
p	0.821	0.999

- VFFC

	1st order	2nd order
ρ	0.667	0.819
u	0.808	0.977
p	0.798	0.996

- VFRoe

	1st order	2nd order
ρ	0.669	0.828
u	0.791	0.975
p	0.796	0.996

- VFRoe ncv (ρ, u, p)

	1st order	2nd order
ρ	0.667	0.840
u	0.805	0.977
p	0.796	0.995

- VFRoe ncv (τ, u, p)

	1st order	2nd order
ρ	0.653	0.809
u	0.822	0.973
p	0.802	0.995

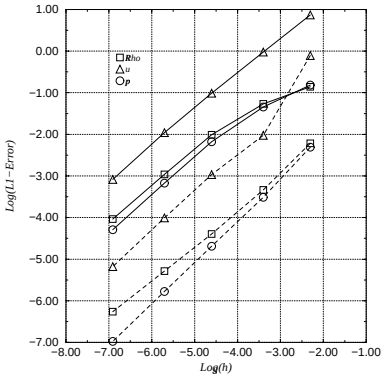

Figure 33: Relaxation d'énergie

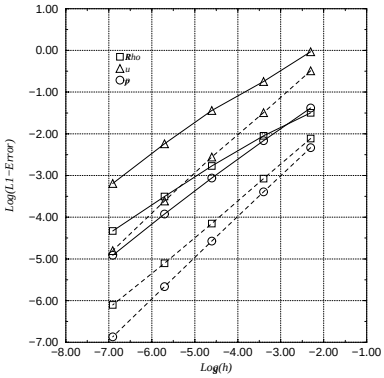

Figure 34: Rusanov

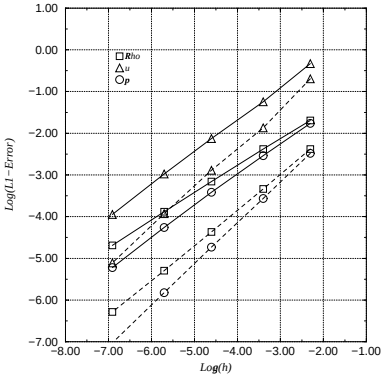

Figure 35: VFFC

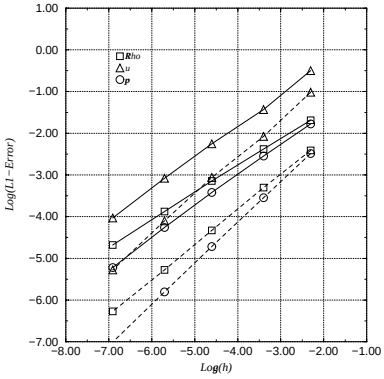

Figure 36: VFRoe

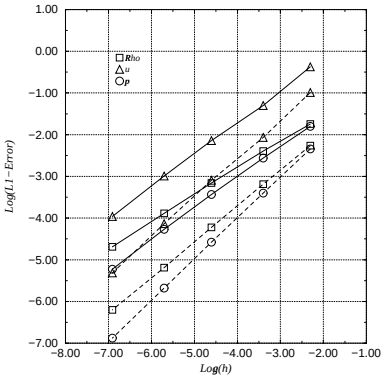

Figure 37: VFRoe ncv (ρ, u, p)

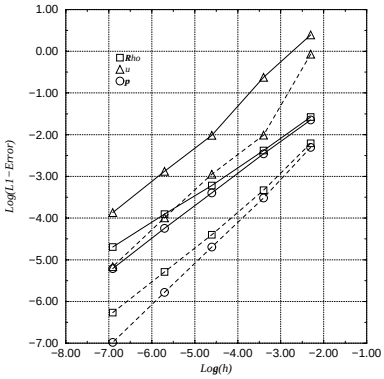

Figure 38: VFRoe ncv (τ, u, p)

Perfect gas EOS - Symmetrical double rarefaction wave

- Energy relaxation

	1st order	2nd order
ρ	0.771	0.998
u	0.785	0.999
p	0.775	0.999

- Rusanov

	1st order	2nd order
ρ	0.773	0.999
u	0.787	1.000
p	0.777	0.999

- VFFC

	1st order	2nd order
ρ	0.768	0.998
u	0.782	1.000
p	0.772	0.999

- VFRoe

	1st order	2nd order
ρ	0.771	0.998
u	0.785	0.999
p	0.775	0.999

- VFRoe ncv (ρ, u, p)

	1st order	2nd order
ρ	0.771	0.998
u	0.785	0.999
p	0.775	0.999

- VFRoe ncv (τ, u, p)

	1st order	2nd order
ρ	0.771	0.998
u	0.785	0.999
p	0.775	0.999

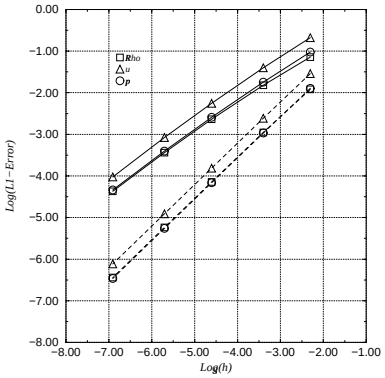

Figure 39: Relaxation d'énergie

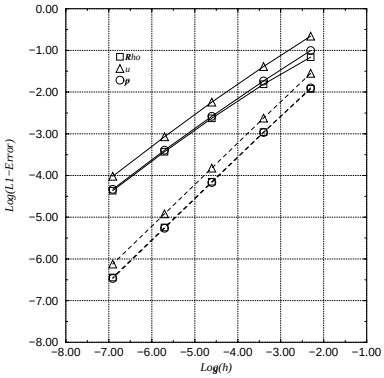

Figure 40: Rusanov

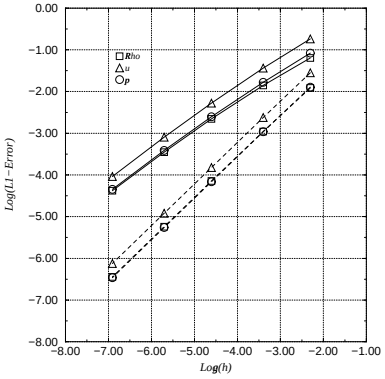

Figure 41: VFFC

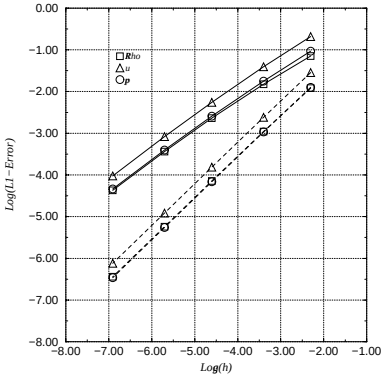

Figure 42: VFRoe

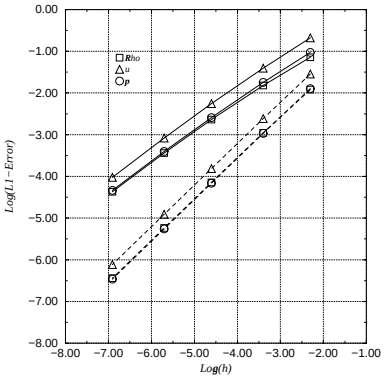

Figure 43: VFRoe ncv (ρ, u, p)

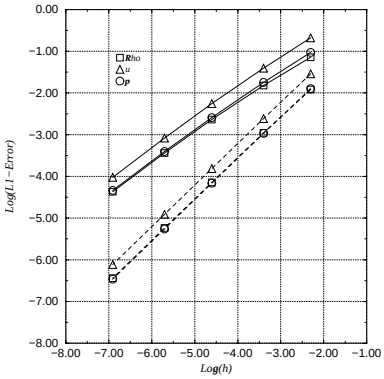

Figure 44: VFRoe ncv (τ, u, p)

Perfect gas EOS - Symmetrical double shock wave

- Energy relaxation

	1st order	2nd order
ρ	1.062	0.935
u	1.157	1.156
p	1.050	1.017

- Rusanov

	1st order	2nd order
ρ	1.060	1.028
u	1.056	1.115
p	0.996	1.001

- VFFC

	1st order	2nd order
ρ	1.060	0.905
u	1.157	1.154
p	1.049	1.019

- VFRoe

	1st order	2nd order
ρ	1.063	0.927
u	1.157	1.153
p	1.050	1.019

- VFRoe ncv (ρ, u, p)

	1st order	2nd order
ρ	1.063	0.929
u	1.158	1.154
p	1.050	1.019

- VFRoe ncv (τ, u, p)

	1st order	2nd order
ρ	1.062	0.947
u	1.157	1.153
p	1.050	1.019

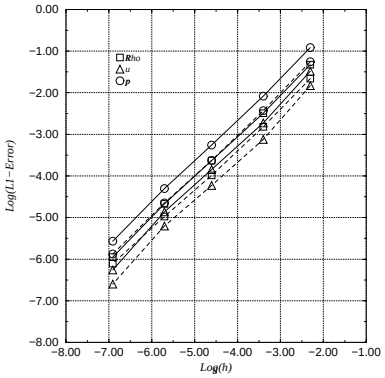

Figure 45: Relaxation d'énergie

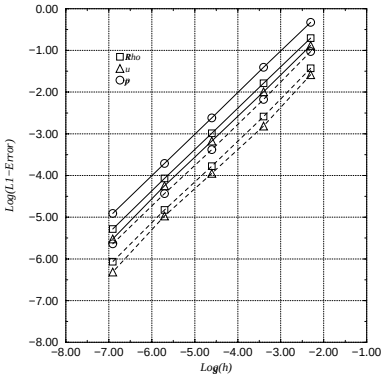

Figure 46: Rusanov

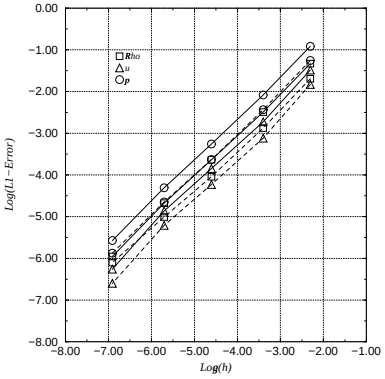

Figure 47: VFFC

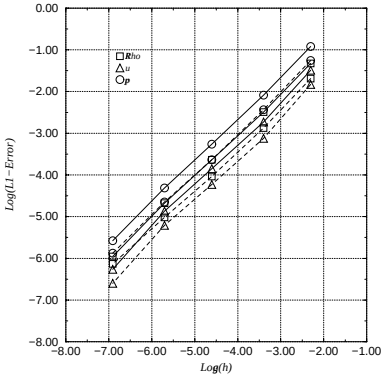

Figure 48: VFRoe

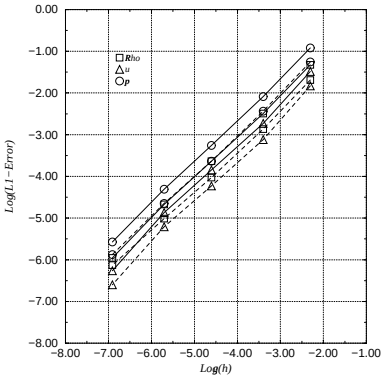

Figure 49: VFRoe ncv (ρ, u, p)

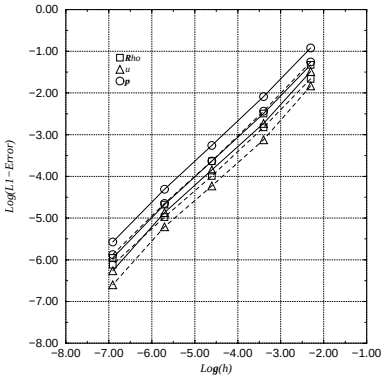

Figure 50: VFRoe ncv (τ, u, p)

4 Conclusion

Several approximate Riemann solvers have been compared in this study. Some among them are based on an approximate Godunov scheme, applying various changes of variables in order to compute approximate values of state at the interface. These make use of conservative variable W, flux variable $F(W)$ or variable (ρ, u, p) or (τ, u, p). The latter enables to preserve unsteady contact discontinuites provided the EOS agrees with some conditions (perfect gas EOS, Tammann EOS belong to the latter class). The practical or theorical behaviour of these schemes when computing steady shock wave, steady contact discontinuity, or vacuum has been investigated. All schemes perform rather well in all experiments, except in vacuum occurence or propagation over vacuum. One drawback of the VFFC scheme can be emphasized : when computing a double supersonic rarefaction wave (with or without vacuum occurence), this scheme blows up after a few time steps. Concerning VFRoe ncv (τ, u, p) and PVRS schemes, changing slightly the average state can increase their robustness and accuracy. The energy relaxation method applied with VFRoe ncv (τ, u, p) scheme has been computed too. The behaviour of this method is nearly the same as the original VFRoe ncv (τ, u, p) scheme. However, the energy relaxation method makes vanish non entropic shocks. The Rusanov scheme provides good results too, though it is slightly less accurate than other schemes investigated, due to important numerical diffusion. But the Rusanov scheme converges as fast as other schemes (in terms of mesh size exponent in the error norm). Moreover, it is the most robust scheme computed here, in particular in test cases with vacuum.

The framework of this paper has been restricted to the computation by Finite Volume schemes of a conservative and hyperbolic system, in one space dimension. Let us recall some extensions of methods used here, in different applications.

Of course, all schemes presented herein can be extended to 2D or 3D problems (see [4]). Rusanov (see [45]), Godunov (see [45]), VFFC (see [2]) and VFRoe ncv (τ, u, p) (see [9]) schemes have been applied to Euler equations with real gas EOS, Shallow Water equations (see [7]) and compressible gas-solid two phase flows (see [11]), with structured or unstructured meshes. Since these systems stay unchanged under frame rotation, a multidimensional framework may rely on a one dimension method (see [20]).

Some systems arising in CFD cannot be written under a conservative form, and thus, approximate jump relations must be proposed (see [14] and [10]). Some of the previous schemes have been extended to the non conservative formalism : Godunov (see [16]), Roe (see [3], [23], [24], [38]), VFRoe ncv (see [5], [8], [45]) and VFRoe (see [31], [1]).

Others non conservative systems are conditionnally hyperbolic, in particular focusing two fluid two phase flows (see [37]). Three main directions have been proposed up to now in the literature. The first consists in splitting the jacobian matrix in several matrices, which may be diagonalised in $\mathbb{R}$ (see [12]). The second way consists in using the sign of the real part of eigenvalues to choose

the flux direction (see [33] and [2]). A third approach is based on a development in power series of eigenvalues and eigenvectors in terms of a small parameter (see [38], [43]).

A Numerical preservation of velocity and pressure through the contact discontinuity in Euler equations

We discuss in this appendix about schemes and state laws, in order to preserve velocity and pressure on the contact discontinuity, in a one dimension framework. We focus on initial conditions of a Riemann problem, with constant velocity and constant pressure. Schemes investigated here can be derived from the formalism of VFRoe ncv scheme, with variable :

$$Y = {}^t(\varphi, u, p)$$

where $\varphi = \varphi(\rho, s)$ (s denotes the specific entropy) must be independant of pressure p (for instance $\varphi = \rho, \tau, ...$).

Restricting to regular solutions, Euler equations can be written related to $Y = {}^t(\varphi, u, p)$ as follows :

$$Y_{,t} + A(Y)Y_{,x} = 0$$

where :

$$A = \begin{pmatrix} u & \rho\varphi_{,\rho} & 0 \\ 0 & u & \rho^{-1} \\ 0 & \hat{\gamma}p & u \end{pmatrix}$$

At each interface, we linearize the matrix $A(Y)$ to obtain a linear Riemann problem, which may be easily solved. Initial conditions are defined by the average values in cells apart from the considered interface ($i + \frac{1}{2}$ for instance) :

$$\begin{cases} \dfrac{\partial Y}{\partial t} + A(\hat{Y})\dfrac{\partial Y}{\partial x} = 0 \\ Y(x,0) = \begin{cases} Y_L = Y(W_i^n) & \text{if } x < 0 \\ Y_R = Y(W_{i+1}^n) & \text{if } x > 0 \end{cases} \end{cases} \tag{10}$$

with $\hat{Y}$ such that $\hat{Y}(Y, Y) = Y$.
To compute the solution at the interface, we need to write the eigenstructure of the matrix A(Y). As usual, the eigenvalues are (c stands for the sound speed) :

$$\lambda_1 = u - c,\ \lambda_2 = u,\ \lambda_3 = u + c$$

The associated right eigenvectors are :

$$r_1(Y) = \begin{pmatrix} \rho\varphi_{,\rho} \\ -c \\ \rho c^2 \end{pmatrix},\ r_2(Y) = \begin{pmatrix} 1 \\ 0 \\ 0 \end{pmatrix},\ r_3(Y) = \begin{pmatrix} \rho\varphi_{,\rho} \\ c \\ \rho c^2 \end{pmatrix}$$

Left eigenvectors of $A(Y)$ are :

$$l_1(Y) = \frac{1}{2c^2}\begin{pmatrix} 0 \\ -c \\ \rho^{-1} \end{pmatrix},\ l_2(Y) = \frac{1}{c^2}\begin{pmatrix} 1 \\ 0 \\ -\varphi_{,\rho} \end{pmatrix},\ l_3(Y) = \frac{1}{2c^2}\begin{pmatrix} 0 \\ c \\ \rho^{-1} \end{pmatrix}$$

In the following, we denote $\tilde{}$ variables computed on the basis of $\overline{Y}$. The solution of the linear problem (10) is :

$$\begin{aligned} Y^*\left(\frac{x}{t}; Y_L, Y_R\right) &= Y_L + \sum_{\frac{x}{t}<\widetilde{\lambda_k}} ({}^t\widetilde{l_k}.(Y_R - Y_L))\widetilde{r_k} \\ &= Y_R - \sum_{\frac{x}{t}>\widetilde{\lambda_k}} ({}^t\widetilde{l_k}.(Y_R - Y_L))\widetilde{r_k} \end{aligned}$$

Since the three eigenvalues of the linear system are distinct, two intermediate states Y_1 and Y_2 may occur :

$$\begin{aligned} Y_1 &= Y_L + \widetilde{\alpha_1}\widetilde{r_1} \\ Y_2 &= Y_R - \widetilde{\alpha_3}\widetilde{r_3} \end{aligned}$$

with :

$$\begin{aligned} \widetilde{\alpha_1} &= -\frac{1}{2\tilde{c}}\Delta u + \frac{1}{2\tilde{\rho}\tilde{c}^2}\Delta p \\ \widetilde{\alpha_3} &= \frac{1}{2\tilde{c}}\Delta u + \frac{1}{2\tilde{\rho}\tilde{c}^2}\Delta p \end{aligned}$$

where $\Delta(.) = (.)_R - (.)_L$. Note that the two intermediate states Y_1 and Y_2 do not depend on the choice of φ.
Recall that initial conditions investigated herein are unsteady contact discontinuity. Thus :

$$\begin{aligned} \Delta u = \Delta p = 0 &\Rightarrow \widetilde{\alpha_1} = \widetilde{\alpha_3} = 0 \\ &\Rightarrow Y_1 = Y_L \text{ and } Y_2 = Y_R \end{aligned}$$

Note that these equalities are verified at each interface of the mesh. Hence, if we denote $\rho_{i+\frac{1}{2}}$ the numerical density of the problem (10) at the interface $i+\frac{1}{2}$, u_0 and p_0 initial velocity and pressure, the Finite Volume scheme applied to the mass conservation equation gives :

$$\begin{aligned} \rho_i^{n+1} &= \rho_i^n - \frac{\Delta t}{\Delta x}((\rho u)_{i+\frac{1}{2}} - (\rho u)_{i-\frac{1}{2}}) \\ &= \rho_i^n - \frac{\Delta t}{\Delta x}u_0(\rho_{i+\frac{1}{2}} - \rho_{i-\frac{1}{2}}) \end{aligned}$$

Now, if we apply the Finite Volume scheme to the momentum conservation equation, it gives :

$$(\rho u)_i^{n+1} = (\rho u)_i^n - \frac{\Delta t}{\Delta x}((\rho u^2 + p)_{i+\frac{1}{2}} - (\rho u^2 + p)_{i-\frac{1}{2}})$$

$$
\begin{aligned}
&= (\rho u)_i^n - \frac{\Delta t}{\Delta x}((\rho_{i+\frac{1}{2}} u_0^2 + p_0) - (\rho_{i-\frac{1}{2}} u_0^2 + p_0)) \\
&= (\rho u)_i^n - \frac{\Delta t}{\Delta x} u_0^2 (\rho_{i+\frac{1}{2}} - \rho_{i-\frac{1}{2}}) \\
&= u_0 \left(\rho_i^n - \frac{\Delta t}{\Delta x} u_0 (\rho_{i+\frac{1}{2}} - \rho_{i-\frac{1}{2}}) \right) \\
&= u_0 \rho_i^{n+1}
\end{aligned}
$$

Thus, we have $u_i^{n+1} = u_0$, $\forall i \in \mathbb{Z}$.
To study the discrete preservation of pressure, let us write the Finite Volume scheme applied to energy conservation equation :

$$
\begin{aligned}
E_i^{n+1} &= E_i^n - \frac{\Delta t}{\Delta x}((u(E+p))_{i+\frac{1}{2}} - (u(E+p))_{i-\frac{1}{2}}) \\
&= E_i^n - \frac{\Delta t}{\Delta x} u_0 (E_{i+\frac{1}{2}} - E_{i-\frac{1}{2}})
\end{aligned}
$$

Energy is defined by $E = \rho\varepsilon + \frac{1}{2}\rho u^2$. Thus, we have :

$$
(\rho\varepsilon)_i^{n+1} = (\rho\varepsilon)_i^n - \frac{\Delta t}{\Delta x} u_0 ((\rho\varepsilon)_{i+\frac{1}{2}} - (\rho\varepsilon)_{i-\frac{1}{2}})
$$

Let us assume that the equation of state can be written under the form :

$$
\rho\varepsilon = f(p) + b\rho + c \tag{11}
$$

where b and c are real constants, and f a inversible function (for instance perfect gas EOS, Tammann EOS, ...). If we introduce this equation of state in the previous equation, it gives :

$$
\begin{aligned}
(f(p) + b\rho + c)_i^{n+1} &= (f(p) + b\rho + c)_i^n \\
&\quad - \frac{\Delta t}{\Delta x} u_0 ((f(p) + b\rho + c)_{i+\frac{1}{2}} - (f(p) + b\rho + c)_{i-\frac{1}{2}}) \\
f(p_i^{n+1}) + b\rho_i^{n+1} + c &= f(p_0) + b\rho_i^n + c \\
&\quad - \frac{\Delta t}{\Delta x} u_0 ((f(p_0) - f(p_0)) + b(\rho_{i+\frac{1}{2}} - \rho_{i-\frac{1}{2}}) + (c - c)) \\
f(p_i^{n+1}) &= f(p_0)
\end{aligned}
$$

Thus, $p_i^{n+1} = p_0$.

Hence, if a state law can be written under the form (11), then a VFRoe ncv scheme, whose variable is (φ, u, p)-like, maintains velocity and pressure constant.

Moreover, if the contact discontinuity is steady (ie $u_0 = 0$), we can remark that the VFRoe ncv (φ, u, p) scheme preserves pressure and velocity exactly constant, whatever the state law considered.

References

[1] C. Berthon, F. Coquel, J.M. Hérard and M. Uhlmann, An approximate solution of the Riemann problem for a realizable second moment turbulent closure, *submitted in revised form to Shock Waves.*

[2] M. Boucker, *Modélisation numérique multidimensionnelle d'écoulements diphasiques liquide-gaz en régimes transitoire et permanent : méthodes et applications*, PhD thesis, École Normale Supérieure de Cachan, France, December 1998.

[3] G. Brun, J.M. Hérard, D. Jeandel and M. Uhlmann, An approximate roe-type Riemann solver for a class of realizable second order closures, *Int. J. of Comp. Fluid Dyn.*, 2000, vol. 13-3.

[4] T. Buffard, *Analyse de quelques méthodes de volumes finis non structurés pour la résolution des équations d'Euler*, PhD thesis, Université Paris VI, France, 1993.

[5] T. Buffard, T. Gallouët and J.M. Hérard, A naive Godunov scheme to compute a non-conservative hyperbolic system, *Int. Series Num. Math.*, 1998, vol. 129, pp. 129–138.

[6] T. Buffard, T. Gallouët and J.M. Hérard, *Schéma VFRoe en variables caractéristiques. Principe de base et applications aux gaz réels*, EDF-DER Report HE-41/96/041/A, 1996. In French.

[7] ——, A naive Godunov scheme to solve shallow-water equations, *C. R. Acad. Sci. Paris*, 1998, vol. I-326, pp. 885–890.

[8] ——, An approximate Godunov scheme to compute turbulent real gas flow models, *AIAA paper 99-3349*, 1999.

[9] ——, A sequel to a rough Godunov scheme. Application to real gas flows, *Computers and Fluids*, 2000, vol. 29-7, pp. 813–847.

[10] J.F. Colombeau, *Multiplication of distributions*, Springer Verlag, 1992.

[11] L. Combe and J.M. Hérard, *Principe du maximum pour un modèle diphasique gaz-solide à trois équations*, EDF-DER Report HE-41/96/045/A, 1996. In French.

[12] ——, Finite volume algorithm to compute dense compressible gas-solid flows, *AIAA journal*, 1999, vol. 37, pp. 337–345.

[13] F. Coquel and B. Perthame, Relaxation of energy and approximate Riemann solvers for general pressure laws in fluid dynamics equations, *SIAM J. Numer. Anal.*, 1998, vol. 35-6, pp. 2223–2249. In Memory of Ami Harten.

[14] G. Dal Maso, P. Le Floch and F. Murat, Definition and weak stability of non conservative products, *J. Math. Pures Appl.*, 1995, vol. 74, pp. 483–548.

[15] R. Eymard, T. Gallouët and R. Herbin, Finite volume methods, *to appear in Hand book for Numerical Analysis, P.G. Ciarlet & J.L. Lions (Eds.), North-Holland.*

[16] A. Forestier, J.M. Hérard and X. Louis, A Godunov type solver to compute turbulent compressible flows, *C. R. Acad. Sci. Paris*, 1997, vol. I-324, pp. 919–926.

[17] T. Gallouët and J.M. Masella, A rough Godunov scheme, *C. R. Acad. Sci. Paris*, 1996, vol. I-323, pp. 77–84.

[18] B. Gest, J.M. Hérard and L. Kloetzer, *Validation d'un algorithme implicite volumes finis pour gaz réels*, EDF-DER Report HE-41/98/041/A, 1998. In French.

[19] J.M. Ghidaglia, A. Kumbaro and G. Le Coq, Une approche volume fini à flux caractéristiques pour la résolution numérique des systèmes hyperboliques de lois de conservation, *C. R. Acad. Sci. Paris*, 1996, vol. I-322, pp. 981–988.

[20] E. Godlewski and P.A. Raviart, *Numerical analysis for hyperbolic systems of conservation laws*, Springer Verlag, 1996.

[21] S.K. Godunov, A difference method for numerical calculation of discontinous equations of hydrodynamics, *Sbornik*, 1959, pp. 271–300. In Russian.

[22] A. Harten and J.M. Hyman, *A self-adjusting grid for the computation of weak solutions of hyperbolic conservation laws*, Report LA9105, 1981, Center of non linear Studies, Theorical Division, Los Alamos, NM.

[23] J.M. Hérard, *Solveur de Riemann approché pour un système hyperbolique non conservatif issu de la turbulence compressible*, EDF-DER Report HE-41/95/009/A, 1995. In French.

[24] J.M. Hérard, A. Forestier and X. Louis, *A non strictly hyperbolic system to describe compressible turbulence*, EDF-DER Report HE-41/94/011/A, 1994.

[25] A. In, Numerical evaluation of an energy relaxation method for inviscid real fluids, *to appear in SIAM J. Sci. Comp.*

[26] ——, *Méthodes numériques pour les équations de la dynamique des gaz complexes et écoulements diphasiques*, PhD thesis, Université Paris VI, France, October 1999.

[27] M.J. Ivings, D.M. Causon and E.F. Toro, On Riemann solvers for compressible flows, *Int. J. Num. Meth. Fluids*, 1998, vol. 28, pp. 395–418.

[28] R. Kee, J. Miller and T. Jefferson, *Chemkin : a general purpose, problem independant transportable fortran chemical kinetics code package*, SAND Report 80-8003, Sandia National Laboratories.

[29] A. Kumbaro, *Schéma volume fini à flux caractéristiques - implémentation, tests et résultats numériques*, EDF-DER Report HT-30/95/017/A, 1995. In French.

[30] A. Letellier and A. Forestier, *Le problème de Riemann en fluide quelconque*, CEA-DMT Report 93/451, 1993. In French.

[31] J.M. Masella, *Quelques méthodes numériques pour les écoulements diphasiques bi-fluides en conduites pétrolières*, PhD thesis, Université Paris VI, France, May 1997.

[32] J.M. Masella, I. Faille and T. Gallouët, On an approximate Godunov scheme, *Int. J. of Comp. Fluid Dyn.*, 1999, vol. 12, pp. 133–149.

[33] S. Mimouni, M. Boucker, G. Le Coq, J.M. Ghidaglia *et al.*, *An overview of the VFFC-methods and tools for the simulation of two-phase flows*, EDF-DER Report HT-33/99/006/A, 1999.

[34] P. Rascle and O. Morvant, *Interface utilisateur de Thetis - THErmodynamique en Tables d'InterpolationS*, EDF-DER Report HT-13/95021B, 1995. In French.

[35] P.L. Roe, Approximate Riemann solvers, parameter vectors and difference schemes, *J. Comp. Phys.*, 1981, vol. 43, pp. 357–372.

[36] V.V. Rusanov, Calculation of interaction of non-steady shock waves with obstacles, *J. Comp. Math. Phys. USSR*, 1961, vol. 1, pp. 267–279.

[37] L. Sainsaulieu, *Contribution à la modélisation mathématique et numérique des écoulements diphasiques constitués d'un nuage de particules dans un écoulement de gaz*, Thèse d'habilitation, Université Paris VI, France, 1995.

[38] ——, Finite volume approximations of two phase-fluid flows based on approximate Roe-type Riemann solver, *J. Comp. Phys.*, 1995, vol. 121, pp. 1–28.

[39] R. Saurel and R. Abgrall, A simple method for compressible multifluid flows, *SIAM J. Sci. Comp.*, 1999, vol. 21-3, pp. 1115–1145.

[40] N. Seguin, *Comparaison numérique de schémas Volumes Finis pour les équations d'Euler en gaz parfaits et réels*, EDF-DRD Report HI-81/00/010/A, 2000, pp. 1–451. In French.

[41] E.F. Toro, A linearised Riemann solver for time-dependent Euler equations of gas dynamics, *Proc. R. Soc. Lond. A.*, 1991, vol. 434, pp. 683–693.

[42] ——, *Riemann solvers and numerical methods for fluid dynamics*, Springer Verlag, 1997.

[43] I. Toumi and A. Kumbaro, An approximate linearized Riemann solver of a two-fluid model, *J. Comp. Phys.*, 1996, vol. 124, pp. 286–300.

[44] B. Van Leer, Toward the ultimate conservative difference scheme V. A second order sequel to Godunov's method, *J. Comp. Phys.*, 1979, vol. 32, p. 101.

[45] E. Xeuxet, *Comparaison de solveurs numériques pour le traitement de la turbulence bifluide*, PhD thesis, Université d'Evry, France, June 1999.